



# Intestinal MYC modulates obesity-related metabolic dysfunction

Yuhong Luo<sup>1</sup>, Shoumei Yang<sup>1</sup>, Xuan Wu<sup>2,3</sup>, Shogo Takahashi<sup>1,4</sup>, Lulu Sun<sup>1</sup>, Jie Cai<sup>1</sup>, Kristopher W. Krausz<sup>1</sup>, Xiaozhen Guo<sup>5</sup>, Henrique B. Dias<sup>1</sup>, Oksana Gavrilova<sup>6</sup>, Cen Xie<sup>1,5</sup>, Changtao Jiang<sup>1,7</sup>, Weiwei Liu<sup>1,2,3</sup>✉ and Frank J. Gonzalez<sup>1</sup>✉

**MYC is a transcription factor with broad biological functions, notably in the control of cell proliferation. Here, we show that intestinal MYC regulates systemic metabolism. We find that MYC expression is increased in ileum biopsies from individuals with obesity and positively correlates with body mass index. Intestine-specific reduction of MYC in mice improves high-fat-diet-induced obesity, insulin resistance, hepatic steatosis and steatohepatitis. Mechanistically, reduced expression of MYC in the intestine promotes glucagon-like peptide-1 (GLP-1) production and secretion. Moreover, we identify *Cers4*, encoding ceramide synthase 4, catalysing de novo ceramide synthesis, as a MYC target gene. Finally, we show that administration of the MYC inhibitor 10058-F4 has beneficial effects on high-fat-diet-induced metabolic disorders, and is accompanied by increased GLP-1 and reduced ceramide levels in serum. This study positions intestinal MYC as a putative drug target against metabolic diseases, including non-alcoholic fatty liver disease and non-alcoholic steatohepatitis.**

**N**on-alcoholic fatty liver disease (NAFLD), characterized by massive ectopic lipid accumulation in the liver in the absence of substantial alcohol consumption, is becoming the most common chronic and progressive liver disease, paralleling a worldwide increase in obesity fuelled by the dramatic changes in lifestyle and diet during the past century<sup>1</sup>. The global prevalence of NAFLD is currently estimated to be 24% (ref. <sup>2</sup>). NAFLD, particularly its more advanced stage non-alcoholic steatohepatitis (NASH), can progress to end-stage liver diseases such as cirrhosis and hepatocellular carcinoma<sup>3</sup>, and is set to replace viral hepatitis as the leading cause for liver transplantation over the next decade or so, with the disease affecting both adults and children<sup>4</sup>. Despite the rising incidence, no drug has yet been approved for the treatment of NAFLD<sup>5</sup>.

MYC, encoded by proto-oncogene *Myc*, is a highly pleiotropic transcription factor with broad effects on cell proliferation, metabolism, angiogenesis, apoptosis, adhesion and differentiation<sup>6</sup>. Dysregulation of MYC is commonly found in various human cancers<sup>7</sup>. Experimentally, MYC overexpression prompts and MYC inactivation represses tumour development<sup>8–10</sup>. In addition to its role in cancer, MYC is involved in the regulation of metabolic diseases including diabetes and fatty liver diseases. Accumulating studies demonstrate that MYC coordinates glucose homeostasis by regulating glucose transporters, key enzymes in the glycolytic pathway and mitochondrial function, the central feature implicated in insulin resistance and diabetes<sup>11,12</sup>. Transgenic expression of MYC in hepatocytes promoted the progression of alcoholic liver disease via induction of endoplasmic reticulum (ER) stress and inhibition of p53 signalling<sup>13</sup>. Conversely, MYC inactivation in the liver

suppressed ER stress and prevented diet-induced NAFLD<sup>14</sup>. A recent study revealed that MYC cooperated with sterol-regulated element-binding protein 1 (SREBP-1) to promote lipogenesis in hepatic, renal and lung tumour cells<sup>15</sup>. Given that a complete loss of MYC results in embryonic lethality<sup>16</sup>, a previous study with heterozygous *Myc*<sup>+/-</sup> mice showed that reduced expression of MYC increased longevity and enhanced health span, partially through elevated metabolic activity and decreased cholesterol synthesis in the liver<sup>17</sup>. In recent years, the intestine has emerged as a central organ participating in lipid and glucose metabolism<sup>18,19</sup>. However, the effects of intestinal MYC on metabolic diseases have not been investigated.

Herein, intestine-specific *Myc*-disrupted mice were generated and used to clarify the role and dissect the mechanism of intestinal MYC in NAFLD development. Intestinal MYC was induced during obesity and intestine-specific *Myc* disruption ameliorated high-fat diet (HFD)-induced obesity and hepatic steatosis by inducing GLP-1 and suppressing the production and secretion of ceramides. Ceramides are bioactive lipids with various biological effects on insulin resistance, oxidative stress, ER stress, inflammation, energy metabolism and apoptosis<sup>20–23</sup>, which are synthesized through three different pathways: the de novo pathway, the sphingomyelinase pathway and the salvage pathway<sup>24</sup>. *Cers4*, encoding a key enzyme in the de novo pathway, was identified as a new target of MYC in the intestine. Notably, pharmacological inhibition of MYC by 10058-F4 improved diet-induced metabolic disorders, including obesity, hepatic steatosis and fibrosis. This study highlights intestinal MYC as a potential target for the treatment of NAFLD and NASH.

<sup>1</sup>Laboratory of Metabolism, Center for Cancer Research, National Cancer Institute, National Institutes of Health, Bethesda, MD, USA. <sup>2</sup>Department of Laboratory Medicine and Central Laboratory, Shanghai Tenth People's Hospital, Tongji University, Shanghai, P.R. China. <sup>3</sup>Department of Laboratory Medicine, Shanghai Skin Disease Hospital, Tongji University, Shanghai, P.R. China. <sup>4</sup>Department of Biochemistry and Molecular & Cellular Biology, Georgetown University, Washington, DC, USA. <sup>5</sup>State Key Laboratory of Drug Research, Shanghai Institute of Materia Medica, Chinese Academy of Sciences, Shanghai, P.R. China. <sup>6</sup>Mouse Metabolism Core Laboratory, National Institute of Diabetes and Digestive and Kidney Diseases, National Institutes of Health, Bethesda, MD, USA. <sup>7</sup>Department of Physiology and Pathophysiology, School of Basic Medical Sciences, Peking University, Key Laboratory of Molecular Cardiovascular Science, Ministry of Education, Beijing, P.R. China. ✉e-mail: [hsvivian@tongji.edu.cn](mailto:hsvivian@tongji.edu.cn); [gonzalef@mail.nih.gov](mailto:gonzalef@mail.nih.gov)

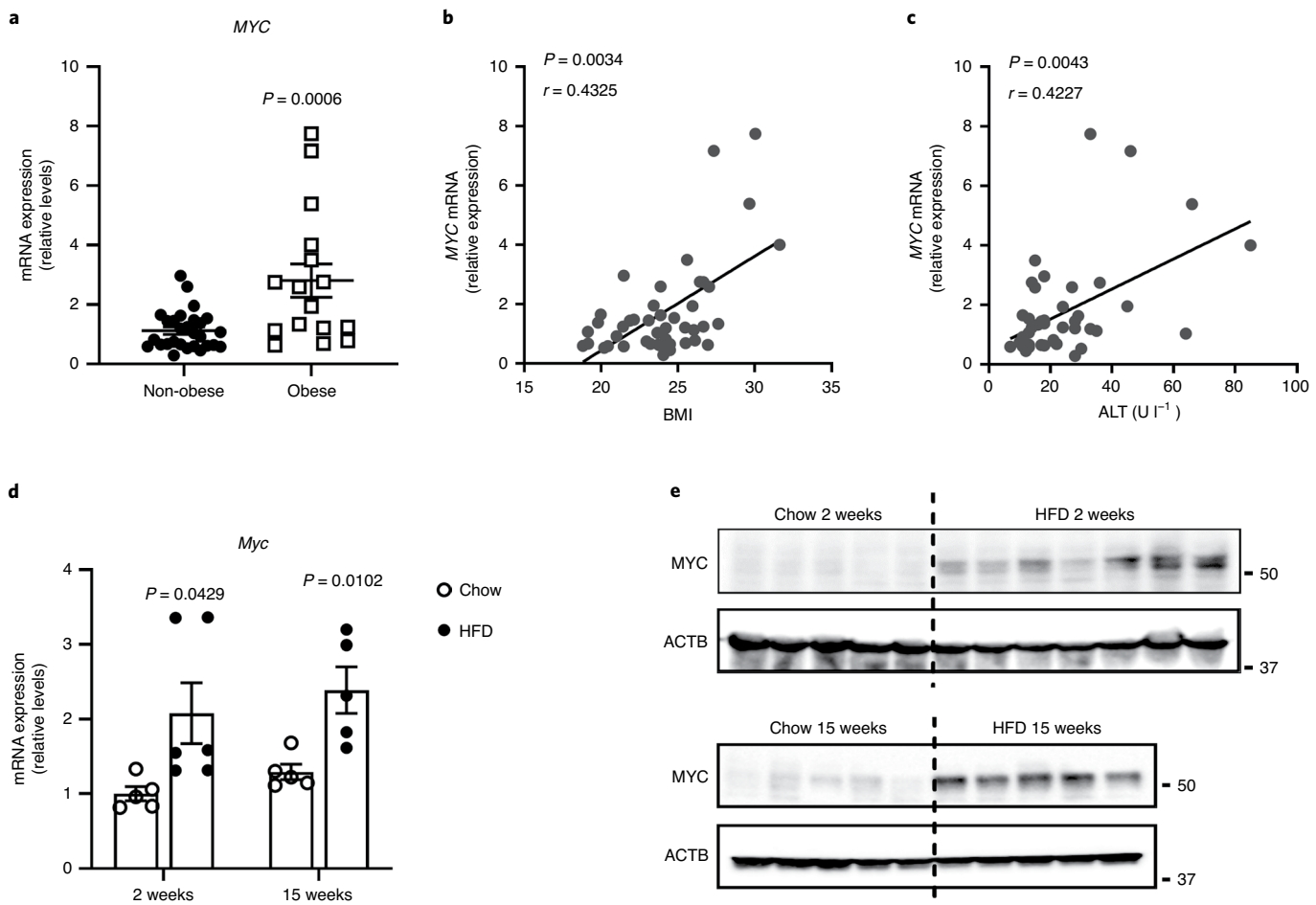


**Fig. 1 | MYC was induced in the intestines of humans and mice with obesity.** **a**, mRNA levels of *MYC* in ileum biopsies from individuals with obesity ( $n=16$ ) or without obesity ( $n=28$ ). **b**, Correlation of *MYC* mRNA levels with BMI;  $n=44$ . **c**, Correlation of *MYC* mRNA levels with serum ALT levels;  $n=44$ . **d**, *Myc* mRNA levels in the intestines of C57BL/6N mice fed a chow diet or HFD for 2 weeks or 15 weeks;  $n=5$  for 2 weeks chow, 15 weeks chow and 15 weeks HFD;  $n=6$  for 2 weeks HFD. **e**, MYC protein levels in the intestines of C57BL/6N mice fed a chow diet or HFD for 2 weeks or 15 weeks. All data are presented as the mean  $\pm$  s.e.m. of biologically independent samples, analysed using a two-tailed Student's *t*-test (**a** and **d**) or a non-parametric Spearman's test (**b** and **c**).

## Results

**Intestinal MYC is induced in humans with obesity.** To investigate the potential association between intestinal MYC and obesity, *MYC* expression was quantified in distal ileum biopsies from individuals with or without obesity. Higher *MYC* expression was observed in humans with obesity relative to non-obese controls (Fig. 1a). The *MYC* mRNA levels in the ileum positively correlated with body mass index (BMI) and serum alanine aminotransferase (ALT) levels

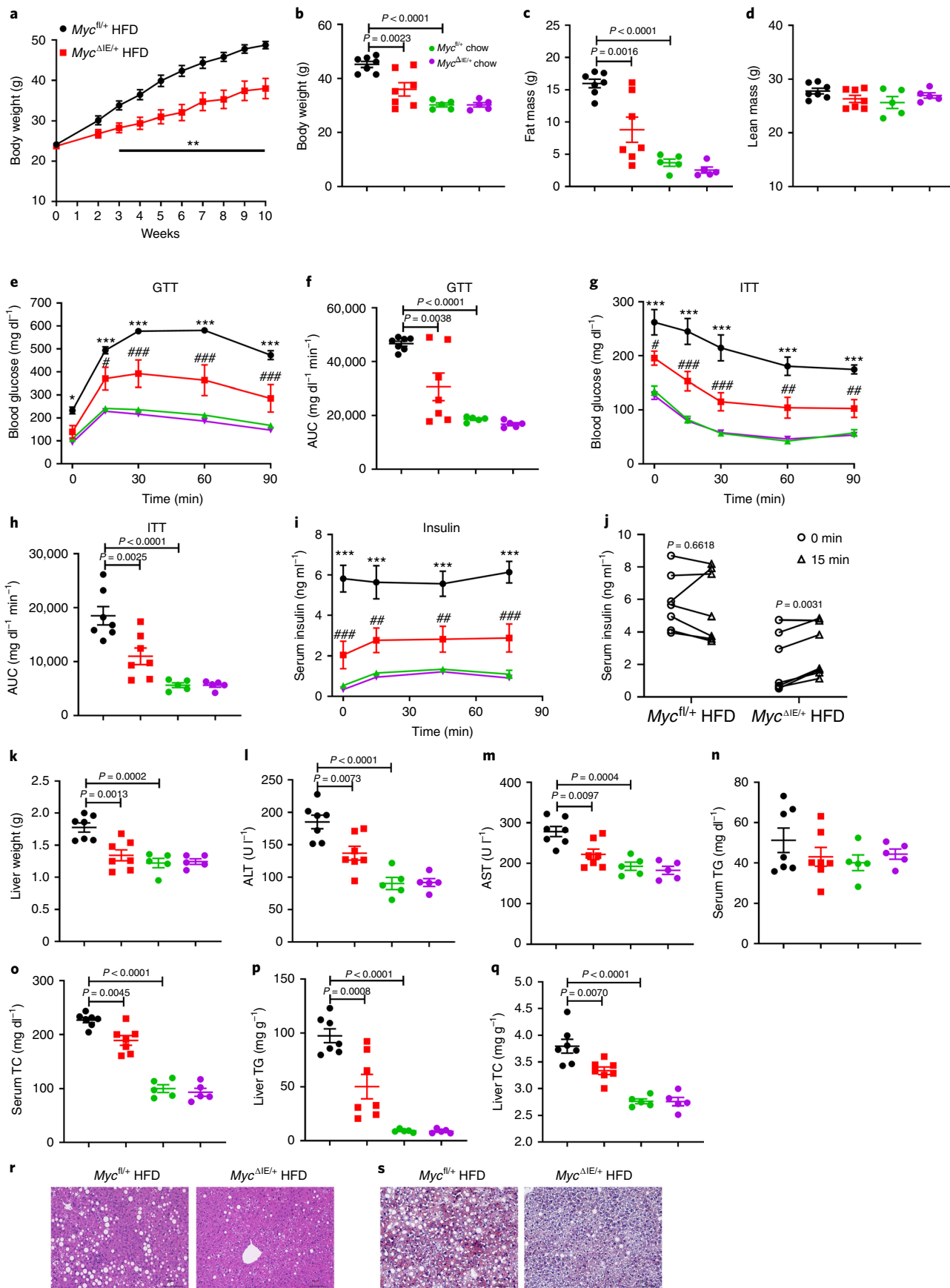
(Fig. 1b,c). Consistent with the human data, a significant induction of intestinal *Myc* mRNA and MYC protein expression was demonstrated as early as 2 weeks following HFD treatment in C57BL/6N mice, an effect that lasted for 15 weeks of long-term HFD treatment (Fig. 1d,e).

**Intestinal MYC reduction improves obesity and fatty liver.** To explore the role of intestinal MYC in metabolic disorders and

**Fig. 2 | *Myc*<sup>ΔIE/+</sup> mice displayed less obesity and hepatic steatosis under HFD challenge.** *Myc*<sup>fl/+</sup> and *Myc*<sup>ΔIE/+</sup> mice were fed a chow diet or HFD for 10 weeks. Data are representative of  $n=3$  experiments. **a**, Body weight curve.  $^{***}P=0.0058$  for 3 weeks,  $P=0.0032$  for 4 weeks,  $P=0.0016$  for 5 weeks,  $P=0.0010$  for 6 weeks,  $P=0.0029$  for 7 weeks,  $P=0.0014$  for 8 weeks,  $P=0.0020$  for 9 weeks and  $P=0.0017$  for 10 weeks. **b**, End point body weight. **c**, Fat mass. **d**, Lean mass. **e**, GTT.  $^*$  or  $^{***}P=0.0230$ ,  $P<0.0001$ ,  $P<0.0001$ ,  $P<0.0001$  and  $P<0.0001$ , from left to right, *Myc*<sup>fl/+</sup> HFD group versus *Myc*<sup>fl/+</sup> chow group.  $^{\#}$  or  $^{###}P=0.0299$ ,  $P=0.0003$ ,  $P<0.0001$  and  $P=0.0002$ , from left to right, *Myc*<sup>ΔIE/+</sup> HFD group versus *Myc*<sup>fl/+</sup> HFD group. **f**, GTT area under the curve (AUC). **g**, ITT.  $^{***}P<0.0001$ ,  $P<0.0001$ ,  $P<0.0001$ ,  $P<0.0001$  and  $P<0.0001$ , from left to right, *Myc*<sup>fl/+</sup> HFD group versus *Myc*<sup>fl/+</sup> chow group.  $^{\#}$  or  $^{##}$  or  $^{###}P=0.0108$ ,  $P=0.0002$ ,  $P<0.0001$ ,  $P=0.0023$  and  $P=0.0047$ , from left to right, *Myc*<sup>ΔIE/+</sup> HFD group versus *Myc*<sup>fl/+</sup> HFD group. **h**, ITT AUC. **i**, Insulin curve in response to glucose.  $^{***}P<0.0001$ ,  $P<0.0001$ ,  $P<0.0001$  and  $P<0.0001$ , from left to right, *Myc*<sup>fl/+</sup> HFD group versus *Myc*<sup>fl/+</sup> chow group.  $^{##}$  or  $^{###}P<0.0001$ ,  $P=0.0012$ ,  $P=0.0020$  and  $P=0.0002$ , from left to right, *Myc*<sup>ΔIE/+</sup> HFD group versus *Myc*<sup>fl/+</sup> HFD group. **j**, insulin levels at 0 min and 15 min after glucose load. **k**, Liver weight. **l**, Serum ALT. **m**, Serum AST. **n**, Serum triglyceride (TG). **o**, Serum total cholesterol (TC). **p**, Hepatic triglyceride. **q**, Hepatic total cholesterol. In **a–q**,  $n=5$  for chow and  $n=7$  for HFD. All data are presented as the mean  $\pm$  s.e.m. of biologically independent samples, analysed using a two-tailed Student's *t*-test (**a**), a two-tailed paired *t*-test (**j**), one-way ANOVA followed by Tukey's multiple-comparisons test (**b–d**, **f**, **h** and **k–q**) or two-way ANOVA followed by Tukey's multiple-comparisons *t*-test (**e**, **g** and **i**). **r,s**, Representative H&E staining (**r**) and ORO staining (**s**) of liver sections ( $n=4$  mice per group, three images per mouse per staining). Scale bar, 100  $\mu$ m.

NAFLD, an intestine-specific *Myc*-disrupted mouse line villin-cre *Myc*<sup>fl/fl</sup> (*Myc*<sup>ΔIE</sup>) was generated by crossing the *Myc*<sup>fl/fl</sup> mice with villin-cre transgenic mice. However, homozygous loss of MYC in

the intestine was lethal because all the pups died within 1 week after weaning (21–28 d of age). *Myc*<sup>ΔIE</sup> mice and their control littermate *Myc*<sup>fl/fl</sup> mice at 21 d of age were analysed, revealing complete loss of



*Myc* mRNA and MYC protein expression in the intestine, with no compensatory increase of *Mycl* or *Mycn* mRNAs (Extended Data Fig. 1q,r). *Myc*<sup>ΔIE</sup> mice were smaller and had lower liver weight than *Myc*<sup>fl/fl</sup> mice (Extended Data Fig. 1a,e,f). The total lengths of the small intestine and colon were shorter, while the relative lengths (normalized to body weight) of the small intestine and colon were longer in *Myc*<sup>ΔIE</sup> mice compared to *Myc*<sup>fl/fl</sup> mice (Extended Data Fig. 1g–j), suggesting compensation. The morphology of the intestines from *Myc*<sup>ΔIE</sup> mice was abnormal with shorter villi–crypt length and reduction of goblet cells (Extended Data Fig. 1b–d). Because Notch signalling plays important roles in intestinal homeostasis and cell fate decisions by lateral inhibition<sup>25,26</sup>, the mRNA and protein levels of Notch and its target genes were examined. In *Myc*<sup>ΔIE</sup> mice, although *Notch1* mRNA levels remained unchanged compared to those in *Myc*<sup>fl/fl</sup> mice, Notch signalling was repressed with reduced levels of cleaved Notch1, Notch target genes *Hes1* and *Rbpj* and Notch ligand *Dll4* (Extended Data Fig. 1q,r). Atoh1 is the key transcription factor responsible for secretory cell fate determination, and is directly inhibited by *Hes1* (ref. <sup>26</sup>). Surprisingly, both Atoh1 and *Hes1* were decreased in intestine depleted of *Myc*, at both the mRNA and protein levels (Extended Data Fig. 1q,r). Intestinal stem cell markers *Lgr5* and *Olfm4* were significantly decreased in *Myc*<sup>ΔIE</sup> mice (Extended Data Fig. 1q), suggesting a shrinkage of the stem cell pool, which might contribute to the shorter villi–crypt length and reduction of goblet cells in *Myc*<sup>ΔIE</sup> mice. Hepatic and serum triglyceride and cholesterol levels, and serum ALT and aspartate aminotransferase (AST) levels were similar between the two genotypes (Extended Data Fig. 1k–p).

Because *Myc*<sup>ΔIE</sup> mice died before adulthood, villin-cre *Myc*<sup>fl/fl</sup> (*Myc*<sup>ΔIE/+</sup>) heterozygous mice with reduced MYC expression in the intestine were generated. The mRNA and protein levels of MYC were reduced in the intestines of *Myc*<sup>ΔIE/+</sup> mice compared to those of *Myc*<sup>fl/fl</sup> mice, but not in extra-intestinal tissues, with no compensatory increase of *Mycl* or *Mycn* mRNAs (Extended Data Fig. 2a–c). The mRNA expression of genes involved in Notch signalling and stem cell marker *Lgr5* was not changed in the intestines of *Myc*<sup>ΔIE/+</sup> mice (Extended Data Fig. 2b), suggesting normal stemness and lineage differentiation. The morphology of the small intestine and intestinal cell proliferation were similar between *Myc*<sup>ΔIE/+</sup> mice and *Myc*<sup>fl/fl</sup> mice as indicated by H&E staining (Extended Data Fig. 2d) and bromodeoxyuridine (BrdU) staining (Extended Data Fig. 2k,l), respectively, with comparable numbers of goblet cells, Paneth cells and enteroendocrine cells (Extended Data Fig. 2e–j). The body weights and liver weights of *Myc*<sup>fl/fl</sup> and *Myc*<sup>ΔIE/+</sup> mice fed a chow diet were similar, without notable changes in glucose tolerance, insulin sensitivity, insulin secretion in response to glucose, serum and hepatic biochemical parameters (Fig. 2b–q).

With HFD challenge, compared to *Myc*<sup>fl/fl</sup> mice, *Myc*<sup>ΔIE/+</sup> mice exhibited less body weight and liver weight gain (Fig. 2a–c,k). Glucose tolerance test (GTT) and insulin tolerance test (ITT) revealed that reduction of MYC in the intestine substantially improved glucose tolerance and insulin sensitivity (Fig. 2e–h). During GTT, *Myc*<sup>ΔIE/+</sup> mice displayed lower serum insulin levels at 0, 15, 45 and 75 min after glucose load than control mice (Fig. 2i). When comparing serum insulin levels at 15 min with the 0-min

time point, we found that *Myc*<sup>ΔIE/+</sup> mice showed increased insulin secretion at 15 min after glucose load, while the changes of insulin in *Myc*<sup>fl/fl</sup> mice were not significant (Fig. 2j), suggesting enhanced insulin secretion in response to glucose in mice with intestinal *Myc* disruption. Hepatic triglyceride levels, hepatic and serum cholesterol levels, and serum ALT and AST levels reflecting hepatic lipotoxicity were markedly lower in *Myc*<sup>ΔIE/+</sup> mice, with no significant difference in serum triglyceride levels as compared to those in *Myc*<sup>fl/fl</sup> mice (Fig. 2l–q). H&E and Oil Red O (ORO) staining showed a reduction in hepatic lipid droplets in *Myc*<sup>ΔIE/+</sup> mice (Fig. 2r,s). Notably, there was no obvious change in the morphology and cell proliferation of the intestines from both genotypes under HFD treatment (Extended Data Fig. 3d). After 18 weeks of HFD feeding, which led to more severe hepatic steatosis, *Myc*<sup>ΔIE/+</sup> mice displayed lower body weight and liver weight gain and less lipid accumulation in the liver than did control mice (Extended Data Fig. 3a–c). Amelioration of these HFD-induced adverse metabolic phenotypes was correlated with reduced mRNA expression of genes involved in lipid synthesis and transport and gluconeogenesis, and increased mRNA expression of genes involved in fatty acid (FA) beta-oxidation and glycolysis in the liver of *Myc*<sup>ΔIE/+</sup> mice compared with *Myc*<sup>fl/fl</sup> mice (Extended Data Fig. 3e,f). Lipid absorption was not affected by intestinal *Myc* disruption as revealed by similar faecal lipid levels in both genotypes fed a HFD (Extended Data Fig. 3g–i). *Myc*<sup>ΔIE/+</sup> mice showed enhanced energy expenditure and higher oxygen consumption than did *Myc*<sup>fl/fl</sup> mice at both 22 °C and 30 °C, without changes in respiratory exchange ratio, food intake or total activity (Extended Data Fig. 3j–n). UCP-1 levels were induced in the subcutaneous white adipose tissue of *Myc*<sup>ΔIE/+</sup> mice (Extended Data Fig. 3o), suggesting enhanced adipose browning.

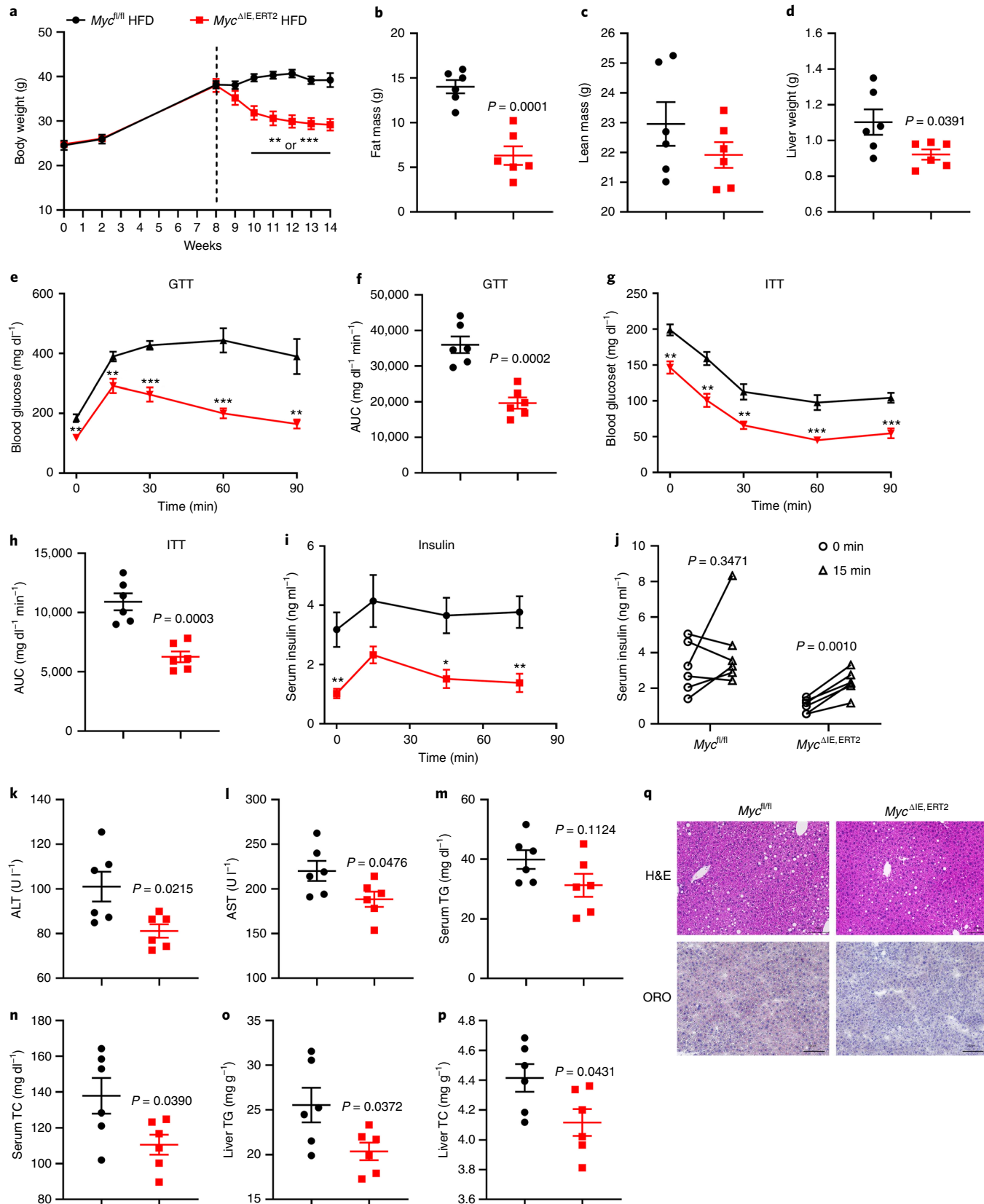
Villin-ERT2-cre *Myc*<sup>fl/fl</sup> (*Myc*<sup>ΔIE,ERT2</sup>) mice were generated by crossing the *Myc*<sup>fl/fl</sup> mice with the villin-ERT2-cre mice to achieve temporal, intestine-specific *Myc* disruption in the presence of tamoxifen. A decrease in *Myc* mRNA was found in the intestines of *Myc*<sup>ΔIE,ERT2</sup> mice compared to *Myc*<sup>fl/fl</sup> mice after tamoxifen treatment, but not in extra-intestinal tissues, with no compensatory increase of *Mycl* or *Mycn* mRNAs (Extended Data Fig. 4a,b). Similarly to the findings in *Myc*<sup>ΔIE/+</sup> mice, the morphology of the small intestine and the numbers of goblet cells, Paneth cells and enteroendocrine cells were comparable between *Myc*<sup>ΔIE,ERT2</sup> mice and *Myc*<sup>fl/fl</sup> mice (Extended Data Fig. 4c–i), without significant changes in the expression of *Lgr5* and Notch pathway-related genes (Extended Data Fig. 4b). MYC was mainly expressed in the nuclei of cells located in the crypt as indicated by immunohistochemistry staining. *Myc*<sup>ΔIE/+</sup> and *Myc*<sup>ΔIE,ERT2</sup> mice showed fewer MYC-positive cells than *Myc*<sup>fl/fl</sup> and *Myc*<sup>ΔIE/+</sup> mice (Extended Data Fig. 5a,b). Consistently, in situ hybridization revealed that *Myc* mRNA was mainly distributed in the crypt area, with less *Myc* mRNA in intestinal *Myc*-disrupted mice compared with control mice (Extended Data Fig. 5c,d).

In mice fed a chow diet, intestinal *Myc* disruption induced by tamoxifen did not affect body weight, liver index, glucose tolerance, insulin sensitivity, serum ALT, serum or hepatic triglyceride or hepatic cholesterol, although serum AST and cholesterol levels were significantly decreased (Extended Data Fig. 5e–n). *Myc*<sup>ΔIE,ERT2</sup>

**Fig. 3 | Intestine-specific inducible *Myc* disruption ameliorated HFD-induced obesity and hepatic steatosis.** *Myc*<sup>fl/fl</sup> and *Myc*<sup>ΔIE,ERT2</sup> mice were first fed a HFD for 8 weeks and then injected weekly with tamoxifen while maintained on HFD for another 6 weeks. Data are representative of  $n=2$  experiments. **a**, Body weight curve. \*\* or \*\*\* $P=0.0012$  for 10 weeks,  $P=0.0003$  for 11 weeks,  $P<0.0001$  for 12 weeks,  $P<0.0001$  for 13 weeks and  $P=0.0006$  for 14 weeks. **b**, Fat mass. **c**, Lean mass. **d**, Liver weight. **e**, GTT. \*\* or \*\*\* $P=0.0021$ ,  $P=0.0066$ ,  $P=0.0001$ ,  $P=0.0003$  and  $P=0.0040$ , from left to right. **f**, GTT AUC. **g**, ITT. \*\* or \*\*\* $P=0.0011$ ,  $P=0.0012$ ,  $P=0.0033$ ,  $P=0.0008$  and  $P=0.0005$ , from left to right. **h**, ITT AUC. **i**, Insulin curve in response to glucose. \* or \*\* $P=0.0052$ ,  $P=0.0104$  and  $P=0.0033$ , from left to right. **j**, Insulin levels at 0 min and 15 min after glucose load. **k**, Serum ALT. **l**, Serum AST. **m**, Serum triglyceride. **n**, Serum total cholesterol. **o**, Hepatic triglyceride. **p**, Hepatic total cholesterol. In **a–p**,  $n=6$ . All data are presented as the mean  $\pm$  s.e.m. of biologically independent samples, analysed using a two-tailed Student's *t*-test (**a–i** and **k–p**) or a two-tailed paired *t*-test (**j**). **q**, Representative H&E staining and ORO staining of liver sections ( $n=4$  mice per group, three images per mouse per staining). Scale bar, 100  $\mu$ m.

mice fed a HFD for 8 weeks to establish obesity and then subjected to activation of the *cre* allele while being maintained on the HFD for another 6 weeks showed reduced body weight and liver weight gain (Fig. 3a–d), less hepatic steatosis (Fig. 3q) and better glucose/

insulin tolerance (Fig. 3e–h) than did similarly treated *Myc*<sup>fl/fl</sup> mice. Serum insulin levels were lower, but insulin secretion in response to glucose was increased in *Myc*<sup>ΔIE,ERT2</sup> mice (Fig. 3i,j). Serum ALT and AST, hepatic triglyceride levels and hepatic and serum cholesterol



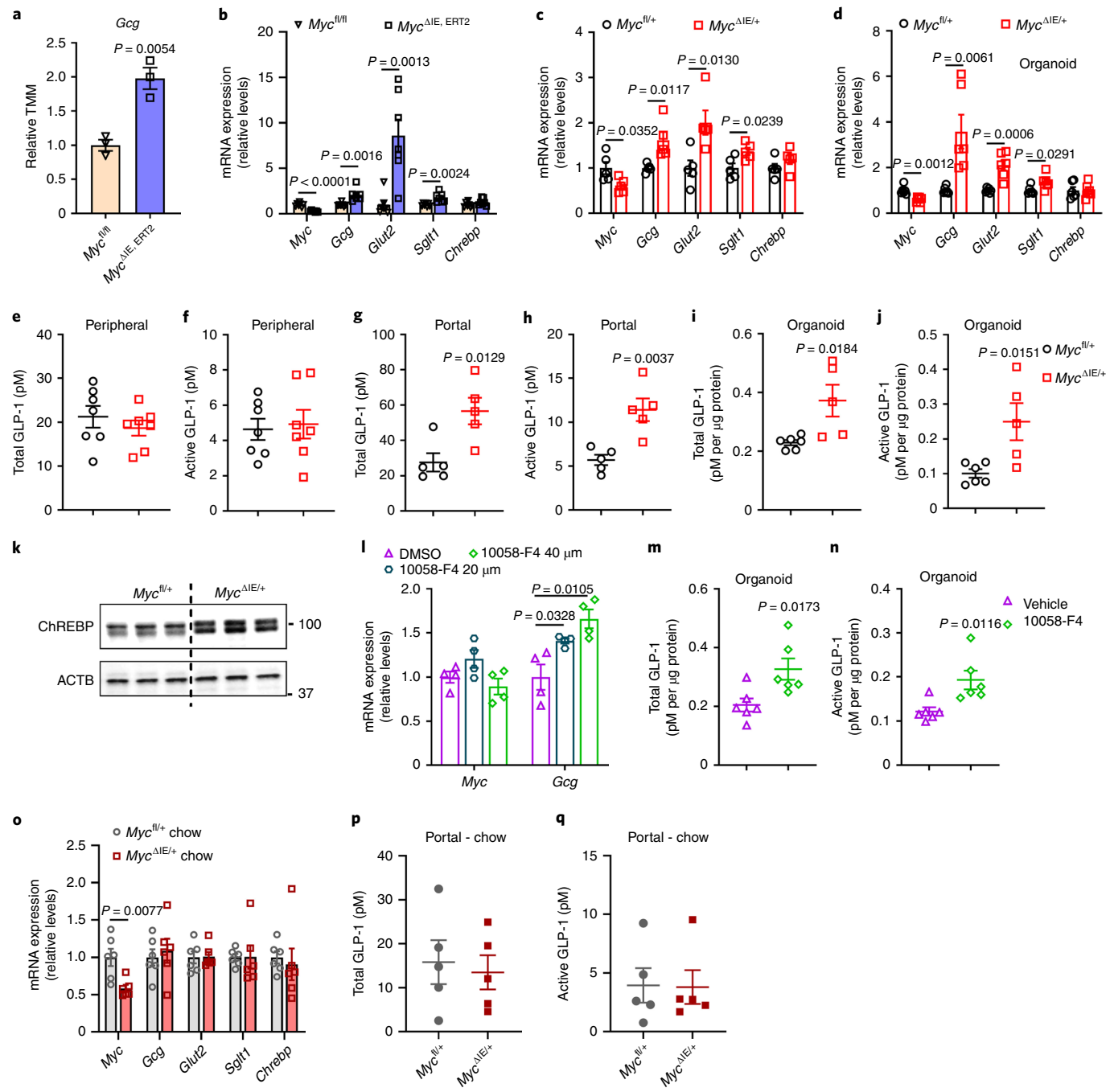


**Fig. 4 | Intestinal Myc disruption or inhibition increased GLP-1 production and secretion.** **a**, Relative TMM of *Gcg* in the intestines of *Myc*<sup>fl/fl</sup> and *Myc*<sup>ΔIE,ERT2</sup> mice injected weekly with tamoxifen and fed a HFD for 2 weeks;  $n=3$ . **b**, mRNA levels of indicated genes in the intestines of *Myc*<sup>fl/fl</sup> and *Myc*<sup>ΔIE,ERT2</sup> mice injected weekly with tamoxifen and fed a HFD for 2 weeks;  $n=7$ . **c**, mRNA levels of indicated genes in the intestines of *Myc*<sup>fl/fl</sup> and *Myc*<sup>ΔIE/+</sup> mice fed a HFD for 2 weeks;  $n=5$ . **d**, mRNA levels of indicated genes in the intestinal organoids isolated from *Myc*<sup>fl/fl</sup> and *Myc*<sup>ΔIE/+</sup> mice fed a HFD for 2 weeks;  $n=6$ . **e,f**, Levels of total GLP-1 (**e**) and active GLP-1 (**f**) in the peripheral blood of *Myc*<sup>fl/fl</sup> and *Myc*<sup>ΔIE/+</sup> mice fed a HFD for 2 weeks;  $n=7$ . **g,h**, Levels of total GLP-1 (**g**) and active GLP-1 (**h**) in the portal vein blood of *Myc*<sup>fl/fl</sup> and *Myc*<sup>ΔIE/+</sup> mice fed a HFD for 2 weeks;  $n=5$ . **i,j**, Levels of total GLP-1 (**i**) and active GLP-1 (**j**) in the culture medium of intestinal organoids isolated from *Myc*<sup>fl/fl</sup> and *Myc*<sup>ΔIE/+</sup> mice fed a HFD for 2 weeks;  $n=6$  for *Myc*<sup>fl/fl</sup> and  $n=5$  for *Myc*<sup>ΔIE/+</sup>. **k**, Protein levels of ChREBP in the intestinal organoids isolated from *Myc*<sup>fl/fl</sup> and *Myc*<sup>ΔIE/+</sup> mice fed a HFD for 2 weeks. **l**, mRNA levels of indicated genes in the intestinal organoids isolated from *Myc*<sup>fl/fl</sup> mice fed a HFD for 2 weeks and treated with vehicle or 20 µM or 40 µM 10058-F4 for 24 h;  $n=4$ . **m,n**, The levels of total GLP-1 (**m**) and active GLP-1 (**n**) in the culture medium of intestinal organoids isolated from *Myc*<sup>fl/fl</sup> mice fed a HFD for 2 weeks and treated with vehicle or 40 µM 10058-F4 for 24 h;  $n=6$ . **o**, mRNA levels of indicated genes in the intestines of *Myc*<sup>fl/fl</sup> and *Myc*<sup>ΔIE/+</sup> mice fed a chow diet;  $n=6$ . **p,q**, Levels of total GLP-1 (**p**) and active GLP-1 (**q**) in the portal vein blood of *Myc*<sup>fl/fl</sup> and *Myc*<sup>ΔIE/+</sup> mice fed a chow diet;  $n=5$ . All data are presented as the mean  $\pm$  s.e.m. of biologically independent samples, analysed using a two-tailed Student's t-test (**a-j** and **l-q**).

levels were substantially lower in *Myc*<sup>ΔIE,ERT2</sup> mice (Fig. 3k-p), indicating that intestinal Myc disruption improved metabolic disorders in mice with established obesity.

To further exclude a decrease in adiposity as a causal factor for the observed beneficial metabolic effects after intestine-specific Myc disruption, *Myc*<sup>ΔIE,ERT2</sup> and *Myc*<sup>fl/fl</sup> mice were injected with tamoxifen

and fed a HFD for 2 weeks that did not lead to a notable change of body weight between the two genotypes (Extended Data Fig. 6a). *Myc*<sup>ΔIE,ERT2</sup> mice exhibited lower serum ALT and AST, less serum and hepatic cholesterol, improved glucose/insulin tolerance and trended towards a reduction in hepatic triglyceride levels, without significant changes in liver weight and serum triglyceride levels, as compared to those in *Myc*<sup>f/f</sup> mice (Extended Data Fig. 6b–j).

**Intestinal Myc disruption promotes GLP-1 secretion.** To explore the potential mechanisms underlying improved metabolic syndrome mediated by intestinal *Myc* disruption, RNA-sequencing (RNA-seq) analysis was carried out with RNAs from the intestines of *Myc*<sup>ΔIE,ERT2</sup> and *Myc*<sup>f/f</sup> mice injected with tamoxifen and fed a HFD for 2 weeks. Principal-component analysis distinguished different expression profiles between *Myc*<sup>ΔIE,ERT2</sup> and *Myc*<sup>f/f</sup> mice (Extended Data Fig. 6k). In total, 343 genes were significantly upregulated and 251 genes were significantly downregulated (fold change > 1.5, adjusted *P* value < 0.05) in the intestines of *Myc*<sup>ΔIE,ERT2</sup> mice compared with *Myc*<sup>f/f</sup> mice (Extended Data Fig. 6l). Kyoto Encyclopedia of Genes and Genomes (KEGG) analysis revealed that sphingolipid metabolism and insulin secretion were among the top pathways affected by intestinal *Myc* disruption (Extended Data Fig. 6m).

GLP-1 is the central factor produced and secreted by the intestines to regulate insulin secretion and systemic glucose homeostasis<sup>27</sup>. The relative trimmed mean of M value (TMM) of *Gcg*, encoding the precursor of GLP-1, was upregulated in HFD-fed *Myc*<sup>ΔIE,ERT2</sup> mice compared with similarly fed *Myc*<sup>f/f</sup> mice (Fig. 4a). An induction of *Gcg* mRNA was confirmed by real-time PCR in *Myc*<sup>ΔIE,ERT2</sup> mice (Fig. 4b) and *Myc*<sup>ΔIE/+</sup> mice (Fig. 4c) fed a HFD, but not in chow-fed *Myc*<sup>ΔIE/+</sup> mice (Fig. 4o). The levels of total GLP-1 and active GLP-1 were increased in the portal vein blood (Fig. 4g,h), but not the peripheral blood (Fig. 4e,f) of HFD-fed *Myc*<sup>ΔIE/+</sup> mice compared with similarly fed *Myc*<sup>f/f</sup> mice, with comparable portal vein GLP-1 levels between the two genotypes fed a chow diet (Fig. 4p,q), which might contribute to enhanced insulin secretion in response to glucose in intestinal *Myc*-disrupted mice under HFD challenge (Figs. 2i,j and 3i,j). Moreover, intestinal organoids isolated from HFD-fed *Myc*<sup>ΔIE/+</sup> mice displayed higher *Gcg* mRNA levels (Fig. 4d), with enhanced total GLP-1 and active GLP-1 secretion in response to glucose (Fig. 4i,j). Glucose stimulates GLP-1 secretion in multiple ways. Two of the main mechanisms are: (1) Na<sup>+</sup>-coupled glucose transport via solute carrier family 5, member 1 (SGLT1) directly depolarizes the membrane to open the Ca<sup>2+</sup> channels and stimulate GLP-1 secretion<sup>28–31</sup> and (2) transport of glucose into cells via solute carrier family 2, member 2 (GLUT2) and subsequent glucose

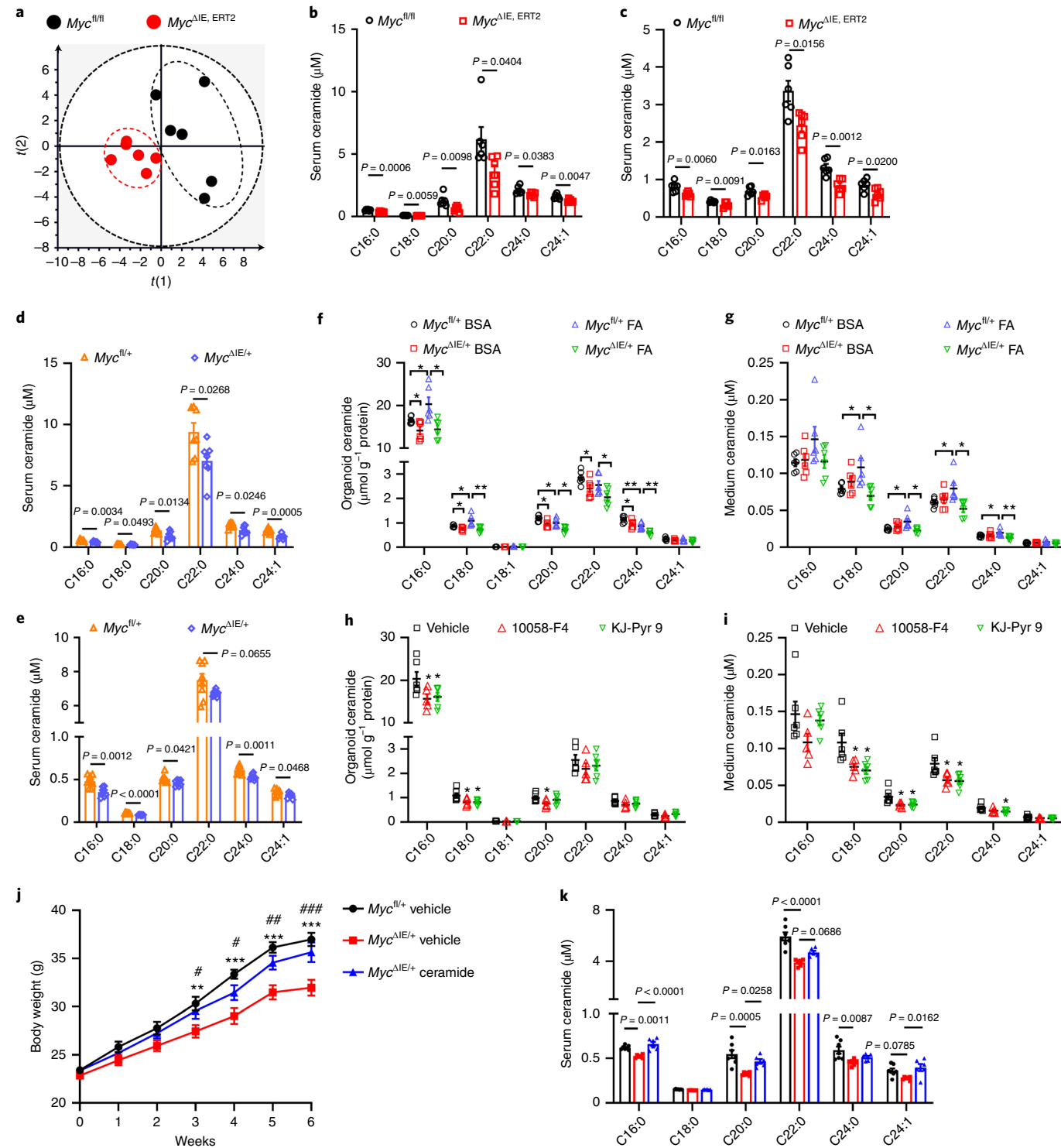
metabolism lead to closure of K<sup>+</sup><sub>ATP</sub>-sensitive channels, resulting in membrane depolarization and Ca<sup>2+</sup> influx and GLP-1 secretion<sup>30–32</sup>. The mRNA levels of *Glut2* and *Sglt1* were upregulated in both the intestines of *Myc*<sup>ΔIE,ERT2</sup> mice (Fig. 4b) and *Myc*<sup>ΔIE/+</sup> mice (Fig. 4c) fed a HFD, and the intestinal organoids isolated from HFD-fed *Myc*<sup>ΔIE/+</sup> mice (Fig. 4d), relative to the controls. MLX interacting protein-like (Mlxipl), also known as carbohydrate-responsive element-binding protein (ChREBP), is a glucose-sensitive transcription factor that regulates *Gcg* expression<sup>33,34</sup>. Although *Chrebp* mRNA was not changed by intestinal *Myc* disruption (Fig. 4b–d), the ChREBP protein levels were increased in intestinal organoids with reduced *Myc* expression (Fig. 4k). Furthermore, treatment with 10058-F4, a MYC inhibitor, on intestinal organoids increased the secretion of total GLP-1 and active GLP-1 in response to glucose, along with elevated *Gcg* mRNA levels (Fig. 4l–n).

**Intestinal Myc disruption decreases ceramide levels.** As implicated by the RNA-seq analysis, sphingolipid metabolism was affected by intestinal *Myc* disruption. To further decipher the underlying mechanism, lipidomics was performed to analyse the metabolites in the serum of *Myc*<sup>ΔIE,ERT2</sup> and *Myc*<sup>f/f</sup> mice injected with tamoxifen and fed a HFD for 18 weeks. Multivariate analysis distinguished different metabolic profiles between the two genotypes (Fig. 5a). Supervised orthogonal projection to latent structures multivariate data analysis (OPLS-DA) was then performed to maximize the difference of metabolic profiles and the variable importance in projection (VIP) score analysis of OPLS-DA revealed that several ceramides, including C16:0, C20:0, C22:0, C24:0 and C24:1, contributed to the separation with VIP scores > 2.0 (Supplementary Table 1). These ceramides were then quantified and found to be substantially lower in the serum of *Myc*<sup>ΔIE,ERT2</sup> mice compared to controls (Fig. 5b). In *Myc*<sup>ΔIE,ERT2</sup> mice first fed a HFD for 8 weeks and then treated with tamoxifen while maintained on HFD for another 6 weeks, and in *Myc*<sup>ΔIE/+</sup> mice fed a HFD for 10 weeks, serum ceramide levels were lower than those in similarly fed controls (Fig. 5c,d). To explore if the reduction of ceramides is an early event with intestinal *Myc* disruption, ceramide levels in serum samples from 2-week HFD-fed mice were measured. The levels of C16:0, C18:0, C20:0, C24:0 and C24:1 were significantly lower, and C22:0 tended to decrease, in the serum of *Myc*<sup>ΔIE/+</sup> mice compared to *Myc*<sup>f/f</sup> mice (Fig. 5e). Intestinal organoids were used to examine the production and secretion of ceramides. Ceramide levels in the culture medium were increased by FA treatment, mimicking the HFD condition, suggesting enhanced ceramide secretion with FA treatment (Fig. 5g). C16:0 and C18:0 levels in the organoids were increased, while levels of

**Fig. 5 | Intestinal Myc disruption reduced ceramide production and secretion.** **a**, Score scatter plot of a principal-component analysis model of serum lipid metabolites between *Myc*<sup>f/f</sup> and *Myc*<sup>ΔIE,ERT2</sup> mice injected weekly with tamoxifen and fed a HFD for 18 weeks; *n* = 6. Each point represents an individual mouse sample. **b**, Ceramide levels in the serum of *Myc*<sup>f/f</sup> and *Myc*<sup>ΔIE,ERT2</sup> mice injected weekly with tamoxifen and fed a HFD for 18 weeks; *n* = 6. **c**, Ceramide levels in the serum of *Myc*<sup>f/f</sup> and *Myc*<sup>ΔIE,ERT2</sup> mice first fed a HFD for 8 weeks and then injected weekly with tamoxifen while maintained on HFD for another 6 weeks; *n* = 6. **d**, Ceramide levels in the serum of *Myc*<sup>f/f</sup> and *Myc*<sup>ΔIE/+</sup> mice fed a HFD for 10 weeks; *n* = 7. **e**, Ceramide levels in the serum of *Myc*<sup>f/f</sup> and *Myc*<sup>ΔIE/+</sup> mice fed a HFD for 2 weeks; *n* = 8. **f,g**, Intestinal organoids were isolated from *Myc*<sup>f/f</sup> and *Myc*<sup>ΔIE/+</sup> mice fed a HFD for 2 weeks. The levels of ceramide in the organoids (**f**) and culture medium (**g**) of organoids treated with control BSA or BSA-conjugated FA (0.2 mM palmitic acid + 0.4 mM oleic acid) for 48 h; *n* = 6. *Myc*<sup>f/f</sup> FA versus *Myc*<sup>f/f</sup> BSA, \* or \*\**P* = 0.0480, *P* = 0.0495, *P* = 0.0483, *P* = 0.0061, *P* = 0.0428, *P* = 0.0411, *P* = 0.0474 and *P* = 0.0460, from left to right. *Myc*<sup>ΔIE/+</sup> FA versus *Myc*<sup>ΔIE/+</sup> BSA, \**P* = 0.0263, *P* = 0.0103, *P* = 0.0110, *P* = 0.0419 and *P* = 0.0474, from left to right. *Myc*<sup>ΔIE/+</sup> FA versus *Myc*<sup>f/f</sup> FA, \* or \*\**P* = 0.0102, *P* = 0.0075, *P* = 0.0123, *P* = 0.0493, *P* = 0.0020, *P* = 0.0163, *P* = 0.0199, *P* = 0.0136 and *P* = 0.0081, from left to right. **h,i**, Intestinal organoids were isolated from *Myc*<sup>f/f</sup> mice fed a HFD for 2 weeks. The levels of ceramide in the organoids (**h**) and culture medium (**i**) of organoids treated with BSA-conjugated FA together with vehicle or 40 μM 10058-F4 or 10 μM KJ-Pyr-9 for 48 h; *n* = 6 for vehicle and KJ-Pyr-9 groups; *n* = 5 for 10058-F4 group. 10058-F4 versus vehicle, \**P* = 0.0473, *P* = 0.0483, *P* = 0.0445, *P* = 0.0448, *P* = 0.0441 and *P* = 0.0438, from left to right. KJ-Pyr-9 versus vehicle, \**P* = 0.0487, *P* = 0.0256, *P* = 0.0168, *P* = 0.0348, *P* = 0.0251 and *P* = 0.0377, from left to right. **j,k**, *Myc*<sup>f/f</sup> and *Myc*<sup>ΔIE/+</sup> mice were fed a HFD and injected daily intraperitoneally with vehicle or ceramide for 6 weeks; *n* = 7 for *Myc*<sup>f/f</sup> vehicle group; *n* = 6 for *Myc*<sup>ΔIE/+</sup> vehicle and *Myc*<sup>ΔIE/+</sup> ceramide groups. **j**, Body weight curve. \*\* or \*\*\**P* = 0.0038 for 3 weeks, *P* < 0.0001 for 4–6 weeks, *Myc*<sup>ΔIE/+</sup> vehicle versus *Myc*<sup>f/f</sup> vehicle. # or ## or ###*P* = 0.0462, *P* = 0.0213, *P* = 0.0025 and *P* = 0.0003 for 3–6 weeks, *Myc*<sup>ΔIE/+</sup> ceramide versus *Myc*<sup>ΔIE/+</sup> vehicle. **k**, Serum ceramide levels. All data are presented as the mean ± s.e.m. of biologically independent samples, analysed using a two-tailed Student's *t*-test (**b–i**), two-way ANOVA followed by Dunnett's multiple-comparisons test (**j**) or one-way ANOVA followed by Tukey's multiple-comparisons test (**k**).

C20:0, C22:0, C24:0 and C24:1 were either unchanged or decreased after FA treatment (Fig. 5f). Compared to *Myc*<sup>fl/fl</sup> organoids treated with FA, *Myc*<sup>ΔIE/+</sup> organoids showed lower ceramide levels in both culture medium and organoids under FA treatment, suggesting less ceramide production and secretion in intestines with *Myc* disruption (Fig. 5f,g). Similarly, organoids treated with 10058-F4 or KJ-Pyr-9, two MYC inhibitors, showed lower ceramide levels in both culture medium and organoids compared with vehicle-treated organoids, indicating less ceramide production and secretion with MYC inhibition (Fig. 5h,i).

**Ceramides exacerbate HFD-induced obesity and hepatosteatosis.** To determine if intestinal *Myc* disruption improves NAFLD through ceramide reduction, C16:0 ceramide or vehicle was administered to *Myc*<sup>fl/fl</sup> and *Myc*<sup>ΔIE/+</sup> mice fed a HFD for 6 weeks. *Myc*<sup>ΔIE/+</sup> mice injected with ceramide showed increased ceramide levels in the serum that were comparable to those in vehicle-treated *Myc*<sup>fl/fl</sup> mice (Fig. 5k). Administration of ceramide partially reversed the improvement in body weight (Fig. 5j), liver weight (Extended Data Fig. 7e), hepatic steatosis (Extended Data Fig. 7m) and insulin resistance (Extended Data Fig. 7a-d) in *Myc*<sup>ΔIE/+</sup> mice as compared to



*Myc<sup>fl/+</sup>* mice. Serum cholesterol and hepatic triglyceride and cholesterol levels were increased in ceramide-treated *Myc<sup>ΔIE/+</sup>* mice compared with vehicle-treated *Myc<sup>ΔIE/+</sup>* mice (Extended Data Fig. 7h–k). The reduction of serum ALT and AST levels in *Myc<sup>ΔIE/+</sup>* mice was also abrogated by ceramide administration (Extended Data Fig. 7f,g). Consistent with the elevation in hepatic lipid accumulation, the mRNA expression of genes involved in lipid synthesis were increased, while genes involved in FA beta-oxidation were decreased in the liver of ceramide-treated *Myc<sup>ΔIE/+</sup>* mice compared with vehicle-treated *Myc<sup>ΔIE/+</sup>* mice (Extended Data Fig. 7l).

**Intestinal MYC targets *Cers4* to modulate ceramide synthesis.** Ceramides are synthesized through three different pathways, the de novo pathway from palmitoyl-CoA and serine, the sphingomyelinase pathway from sphingomyelin, and the salvage pathway from complex sphingolipids. The mRNAs encoding genes involved in the three pathways were examined (Fig. 6a–f). Among all the genes examined, the mRNA levels of *Cers4*, encoding ceramide synthase 4 in the de novo pathway, were consistently decreased in intestinal organoids isolated from *Myc<sup>ΔIE/+</sup>* mice compared with *Myc<sup>fl/+</sup>* mice (Fig. 6a), and in intestinal organoids treated with 10058-F4 compared with vehicle-treated organoids (Fig. 6d). Western blot analysis confirmed a reduction of CERS4 protein in the intestinal organoids isolated from *Myc<sup>ΔIE/+</sup>* mice or treated with 10058-F4 (Fig. 6k), and in the intestines of *Myc<sup>ΔIE/+</sup>* mice (Fig. 6l). Intestinal *Cers4* was induced by both short-term and long-term HFD treatment in mice (Extended Data Fig. 8a). Furthermore, the CERS4 mRNA was increased in the ileum biopsies from individuals with obesity relative to non-obese individuals and positively correlated with BMI, ALT levels and MYC mRNA levels (Fig. 6g–j).

Five potential MYC-binding sites, known as enhancer box (Ebox) sequences, were identified within 4.5 kb upstream and 1 kb downstream of the *Cers4* transcription start site (TSS) by Genomatix MatInspector (Fig. 6m). Inserts (A–C) containing the predicted Ebox sites were cloned into the pGL4.11 reporter vectors and luciferase assays were performed. In MC38 cells transfected with pGL4.11-Cers4 B, overexpression of MYC significantly induced the luciferase activity, an effect diminished by adding the MYC inhibitor 10058-F4. The pGL4.11-Cers4 A and pGL4.11-Cers4 C reporter signals were similar to those of the empty vector pGL4.11 (Fig. 6n). MYC binding assessed by chromatin immunoprecipitation coupled with quantitative PCR (ChIP-qPCR) assay revealed an enrichment of *Cers4* promoter region B using primer set B, an effect abolished by adding 10058-F4 (Fig. 6p). *Ccnd2*, encoding cyclin D2, which is a bona fide MYC target gene, served as a positive control for MYC binding (Fig. 6o). Together, these data demonstrate that MYC regulates *Cers4* transcription through direct binding to an Ebox within 500 base pairs upstream of the *Cers4* TSS.

In addition to *Cers4*, intestinal *Myc* disruption significantly decreased the mRNA expression of *Smpd3* (Fig. 6b), although no significant change in *Smpd3* mRNA levels after 10058-F4 treatment was observed (Fig. 6e). Western blot analysis revealed a reduction

of SMPD3 protein in the intestines of *Myc<sup>ΔIE/+</sup>* mice compared to *Myc<sup>fl/+</sup>* mice (Extended Data Fig. 8a), and in the intestines of C57BL/6N mice treated with 10058-F4 compared to vehicle-treated mice (Extended Data Fig. 8b). Four Ebox sites were predicted within 2 kb upstream and 0.5 kb downstream of the *Smpd3* TSS (Extended Data Fig. 8c). Luciferase reporter assays demonstrated an enhanced promoter activity of block A by MYC overexpression (Extended Data Fig. 8d). However, MYC binding to this region was not changed by MYC overexpression or inhibition as revealed by ChIP-qPCR assays (Extended Data Fig. 8e).

Silencing of CERS4 in the intestinal organoids by use of recombinant lentivirus carrying mouse *Cers4* shRNA, decreased *Cers4* mRNA and CERS4 protein expression (Extended Data Fig. 9b,c), along with reduced ceramide levels in both culture medium and organoids (Extended Data Fig. 9d,e). Conversely, overexpression of CERS4 by lentivirus carrying mouse *Cers4* cDNA in the intestinal organoids increased *Cers4* mRNA and CERS4 protein expression (Extended Data Fig. 9f,g), along with blunted lower ceramide levels in both culture medium and organoids from *Myc<sup>ΔIE/+</sup>* mice compared to those from *Myc<sup>fl/+</sup>* mice (Extended Data Fig. 9h,i), suggesting that intestinal MYC modulated ceramide synthesis at least partially via targeting *Cers4*.

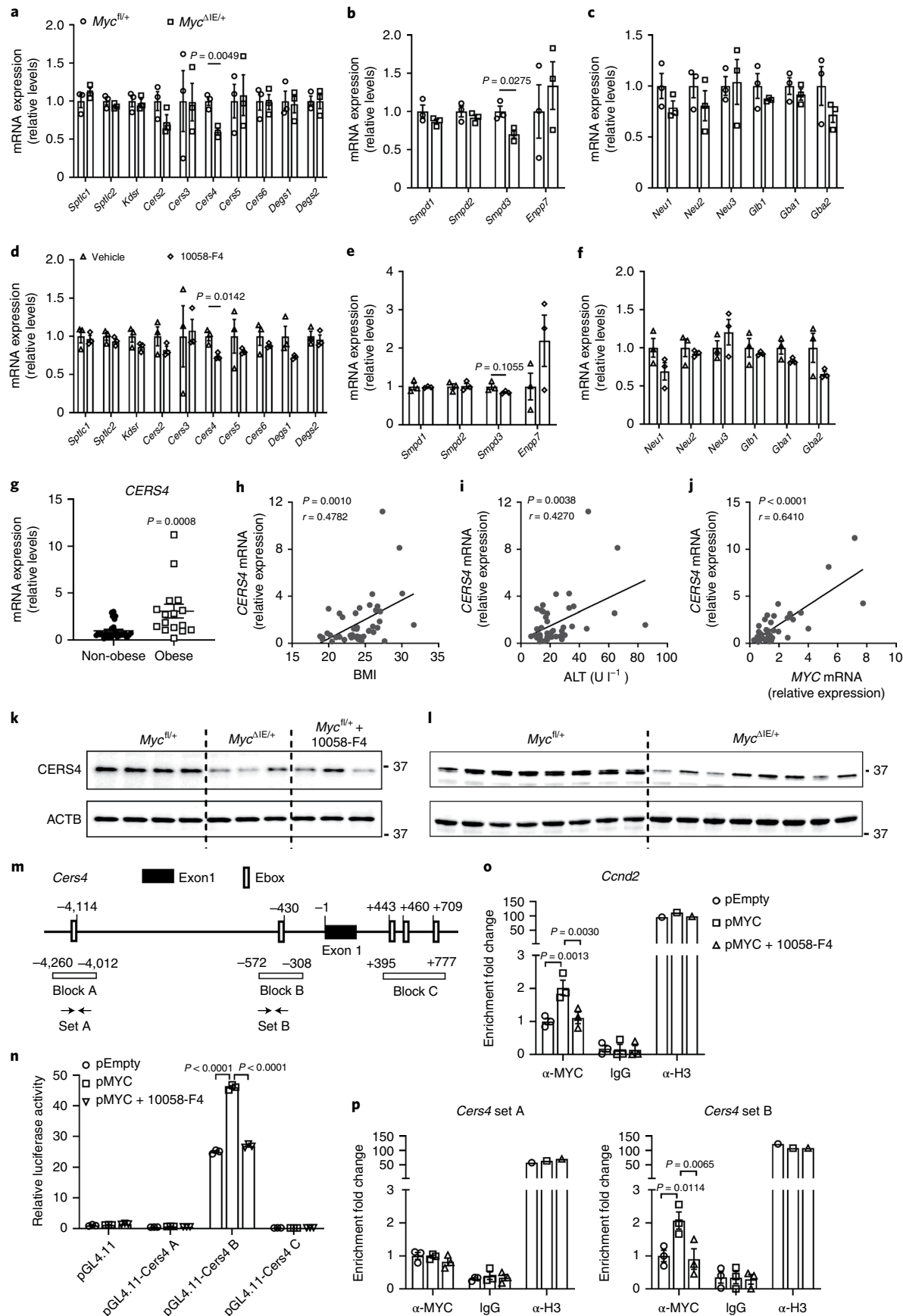
**10058-F4 attenuates hepatic steatosis and fibrosis.** To assess the effect of MYC inhibition on HFD-induced metabolic disorders in vivo, HFD-fed C57BL/6N mice with obesity and hepatic steatosis were treated with vehicle or 10058-F4. Oral administration of 10058-F4 decreased the body weight and liver weight gain (Fig. 7a,b), improved insulin resistance (Fig. 7c–f) and promoted insulin secretion in response to glucose (Fig. 7g,h). Histology analysis revealed reduced hepatic lipid droplets in 10058-F4-treated mice (Fig. 7o). Hepatic triglyceride levels, hepatic and serum cholesterol levels, and serum ALT and AST levels reflecting hepatic lipotoxicity were markedly lower in 10058-F4-treated mice, with no significant difference in serum triglyceride levels as compared to those in vehicle-treated mice (Fig. 7i–n). Intestinal cell proliferation was not affected as indicated by BrdU staining (Fig. 7p). In the liver, 10058-F4 downregulated mRNA expression of *Srebf2* (also known as *Srebp2*), *Scd1*, *Fasn* and *Fabp1*, and upregulated mRNA expression of *Acox1*, *Cyp4a10*, *Cpt2* and *Ehhadh* (Fig. 7w). In addition, 10058-F4 upregulated hepatic mRNA expression of several glycolysis genes and downregulated several gluconeogenesis genes (Fig. 7x,y). The 10058-F4 treatment increased *Gcg* mRNA (Fig. 7r) and ChREBP protein (Fig. 7q) in the intestine, along with elevated total GLP-1 and active GLP-1 levels in the portal vein blood (Fig. 7s,t). The *Cers4* mRNA and CERS4 protein were decreased in the intestines of 10058-F4-treated mice (Fig. 7q,u), resulting in lower serum ceramide levels relative to vehicle-treated mice (Fig. 7v).

To further explore if the effect of 10058-F4 on HFD-induced metabolic syndrome is dependent on intestinal MYC, *Myc<sup>fl/+</sup>* and *Myc<sup>ΔIE/+</sup>* mice were fed a HFD and administered with vehicle or 10058-F4 for 8 weeks. Intestinal *Myc* disruption or 10058-F4

**Fig. 6 | *Cers4* was a MYC target gene in the intestine.** **a–c**, mRNA levels of genes involved in the de novo pathway (**a**), sphingomyelinase pathway (**b**) and salvage pathway (**c**) of ceramide synthesis in the intestinal organoids isolated from *Myc<sup>fl/+</sup>* and *Myc<sup>ΔIE/+</sup>* mice fed a HFD for 2 weeks;  $n=3$ . **d–f**, mRNA levels of genes involved in the de novo pathway (**d**), sphingomyelinase pathway (**e**) and salvage pathway (**f**) of ceramide synthesis in the intestinal organoids isolated from *Myc<sup>fl/+</sup>* mice fed a HFD for 2 weeks and treated with vehicle or 40  $\mu$ M 10058-F4 for 24 h;  $n=3$ . **g**, mRNA levels of CERS4 in ileum biopsies from individuals with obesity ( $n=16$ ) or without obesity ( $n=28$ ). **h**, Correlation of CERS4 mRNA levels with BMI;  $n=44$ . **i**, Correlation of CERS4 mRNA levels with serum ALT levels;  $n=44$ . **j**, Correlation of CERS4 and MYC mRNA levels;  $n=44$ . **k**, Protein levels of CERS4 in the intestinal organoids isolated from *Myc<sup>fl/+</sup>* and *Myc<sup>ΔIE/+</sup>* mice fed a HFD for 2 weeks and treated with vehicle or 40  $\mu$ M 10058-F4 for 48 h. **l**, Protein levels of CERS4 in the intestines of *Myc<sup>fl/+</sup>* and *Myc<sup>ΔIE/+</sup>* mice fed a HFD for 2 weeks. **m**, Schematic of the mouse *Cers4* promoter ( $-4.5\text{ kb}$ ) illustrating the predicted Ebox sites in the regulatory region and the fragments used for luciferase reporter assays. **n**, Luciferase reporter assay of mouse *Cers4* promoter activity;  $n=3$  for  $\alpha$ -MYC and IgG groups;  $n=1$  for  $\alpha$ -H3 group. All data are presented as the mean  $\pm$  s.e.m. of biologically independent samples, analysed using two-tailed Student's *t*-test (**a–g**), non-parametric Spearman's test (**h–j**) or two-way ANOVA followed by Tukey's multiple-comparisons test (**n–p**).

treatment decreased body weight and liver weight gain (Extended Data Fig. 10a–d), improved insulin resistance (Extended Data Fig. 10e–h), promoted insulin secretion in response to glucose

(Extended Data Fig. 10i,j), lowered serum ALT, AST and cholesterol levels (Extended Data Fig. 10k,l,n), and reduced hepatic lipid accumulation (Extended Data Fig. 10o–q). However, *Myc*<sup>ΔIE/+</sup> mice



treated with 10058-F4 did not show further improvement of any of the metabolic parameters examined compared to those in *Myc*<sup>ΔIE/+</sup> mice treated with vehicle (Extended Data Fig. 10a–q), suggesting that the effect of 10058-F4 on HFD-induced metabolic syndrome was mainly dependent on the intact expression of intestinal MYC. Besides, there was no notable change in intestine morphology among the four groups (Extended Data Fig. 10q).

NASH is the advanced stage of NAFLD of great clinical importance with no current therapeutic options. To establish whether intestinal MYC also plays a role in NASH, *Myc*<sup>ΔIE/+</sup> mice and *Myc*<sup>fl/+</sup> mice were subjected to a high-fat, high-cholesterol and high-fructose diet (HFCFD)-induced NASH model. After feeding a HFCFD for 26 weeks, *Myc*<sup>ΔIE/+</sup> mice displayed less body weight and liver weight gain (Fig. 8a,b), lower serum ALT and AST levels (Fig. 8c,d) and improved hepatic steatosis and fibrosis (Fig. 8e) as compared to those in *Myc*<sup>fl/+</sup> mice, paralleled by decreased hepatic expression of mRNAs involved in fibrosis and inflammation (Fig. 8f). To assess the effect of MYC inhibition on NASH, C57BL/6N mice were first fed a HFCFD for 8 weeks and then orally administered vehicle or 10058-F4 daily while they were maintained on the HFCFD for another 12 weeks. Although MYC inhibition had a minor effect on body weight and liver weight (Fig. 8g,h), serum ALT and AST levels and liver fibrosis, as indicated by Sirius red staining, were dramatically decreased by 10058-F4 treatment (Fig. 8i–k). Expression of mRNAs encoded by genes involved in fibrosis and inflammation was significantly decreased in the liver of mice treated with 10058-F4 (Fig. 8l).

## Discussion

In the present study, intestinal MYC is increased with obesity in both mouse and human biopsies. Intestine-specific disruption of *Myc* in *Myc*<sup>ΔIE/+</sup> or *Myc*<sup>ΔIE,ERT2</sup> mice protects against HFD-induced obesity, insulin resistance, hepatic steatosis and fibrosis, accompanied by increased GLP-1 and decreased ceramide levels in serum. Mechanistic studies reveal that reduction of MYC in the intestine increases ChREBP and GLUT2/SGLT1 expression, thus promoting GLP-1 production and secretion. On the other hand, intestinal MYC induces ceramide levels via directly targeting *Cers4*, encoding the key enzyme involved in the de novo synthesis of ceramides. Notably, inhibition of MYC by 10058-F4 exerts therapeutic effects on obesity-related metabolic disorders, suggesting MYC inhibition as a compelling therapeutic strategy for NAFLD/NASH treatment (Fig. 8m).

Previous studies showed that overnutrition, induced by a HFD, could induce intestinal epithelial proliferation by stabilizing β-catenin via increased phosphorylation of glycogen synthase kinase-3β. Activation of the β-catenin pathway promotes expression of downstream genes including *Ccnd1*, encoding cyclin D, that induce intestinal epithelial cell proliferation, which contributes to increased nutrient absorption and obesity development<sup>35,36</sup>. In addition, HFD exposure promotes intestinal stem cell proliferation and

tumorigenicity<sup>37</sup>. Here, intestinal MYC was found to be upregulated in HFD-fed mice compared to chow-fed mice, and in humans with obesity compared to lean counterpart controls. This is likely due to activation of the β-catenin pathway and increased proliferation of intestinal epithelial cells, because *Myc* is a β-catenin target gene and the bona fide key transcription factor regulating the cell cycle<sup>6,38</sup>.

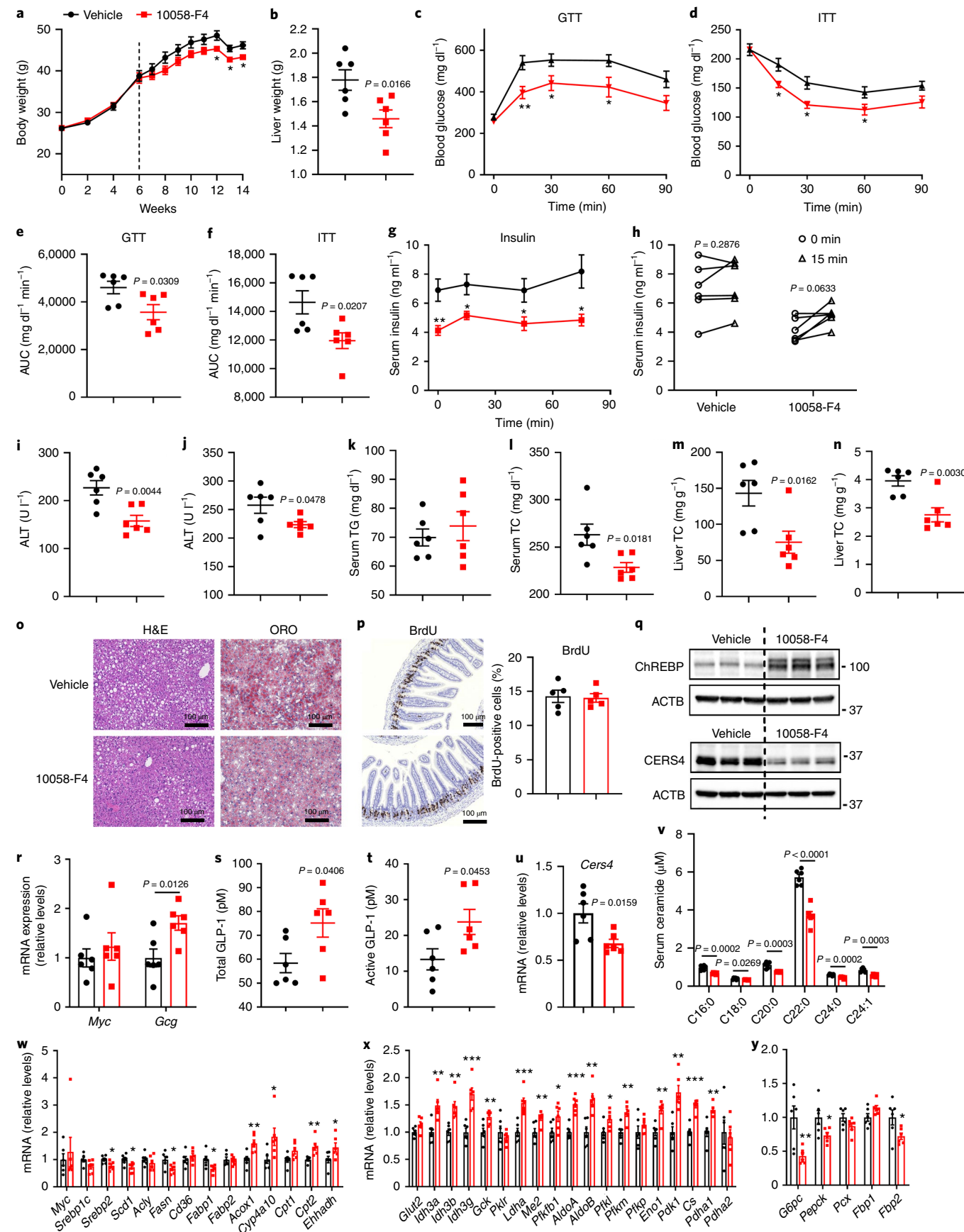
Given the key role of MYC in development, it is not surprising that complete loss of MYC results in embryonic lethality<sup>16</sup>. The intestinal epithelia renew more rapidly than any other tissues in the vertebrate body, replacing the entire intestinal villi every few days. In the present study, homozygous loss of MYC in the intestine was also found to be lethal as all the pups died before reaching adulthood. MYC is mainly expressed in cells in the crypt area, where intestinal stem cells are located. In *Myc*<sup>ΔIE</sup> pups, there was a shrinkage of the intestinal stem cell pool together with shorter villi-crypt lengths, possibly leading to the death of *Myc*<sup>ΔIE</sup> mice. This indicates an indispensable role for MYC in the development and function of the intestine, at least at the early stage of life. MYC was reported to be required for the formation of intestinal crypts but dispensable for the proliferation and homeostasis of intestine epithelium in adult mice<sup>39</sup>. In *Myc*<sup>ΔIE/+</sup> mice, MYC expression was reduced, but not totally lost, allowing for complete viability and metabolic fitness. The remaining MYC was sufficient to maintain normal intestine morphology, cell proliferation and lineage differentiation. Under a chow diet, the body weight of *Myc*<sup>ΔIE/+</sup> mice was similar to that of *Myc*<sup>fl/+</sup> mice, while with HFD challenge, *Myc*<sup>ΔIE/+</sup> mice showed less body weight gain and lipid accumulation in the liver than did *Myc*<sup>fl/+</sup> mice, without changes in intestinal epithelial proliferation, suggesting that intestinal MYC reduction protects against HFD-induced metabolic disorders in a cell proliferation-independent manner.

Transcriptome analysis helped to explore the potential mechanisms underlying improved metabolic syndrome by MYC reduction in the intestine. Insulin secretion is among the top pathways affected by intestinal MYC. GLP-1 is one of the central gut-derived peptide hormones that potentiates insulin secretion and thereby glucose homeostasis<sup>27,40</sup>. Exogenously administered GLP-1 completely normalized blood glucose levels in patients with type 2 diabetes (T2DM)<sup>41,42</sup>, which is the foundation for GLP-1-based treatment of T2DM. GLP-1 exerts its functions through GLP-1 receptor (GLP-1R), which is expressed in various tissues including pancreas, heart, adipose, liver and brain. With the wide distribution of GLP-1R, GLP-1 exhibits multiple effects beyond glucose lowering, including inhibition of appetite and gastric emptying, cardiovascular protection and regulation of hepatic glucose production<sup>27</sup>. Here, *Gcg*, encoding the precursor of GLP-1, was found at increased levels in mice with reduced MYC expression, accompanied by improved insulin resistance and enhanced insulin secretion in response to glucose. Although GLP-1 was reported to enhance satiety and reduce appetite<sup>43,44</sup>, no significant change in food intake was observed in intestinal *Myc*-disrupted mice. A meta-analysis of data from clinical

**Fig. 7 | Inhibition of MYC in the intestine improved HFD-induced hepatic steatosis.** C57BL/6N mice were first fed a HFD for 6 weeks and then administered with vehicle or 10058-F4 while maintained on HFD for another 8 weeks. Data are representative of  $n=3$  experiments. **a**, Body weight curve. \* $P=0.0356$  for 12 weeks,  $P=0.0132$  for 13 weeks and  $P=0.0115$  for 14 weeks. **b**, Liver weight. **c**, GTT. \* or \*\* $P=0.0095$ ,  $P=0.0393$  and  $P=0.0439$ , from left to right. **d**, ITT. \* $P=0.0186$ ,  $P=0.0112$  and  $P=0.0492$ , from left to right. **e**, GTT AUC. **f**, ITT AUC. **g**, Insulin curve in response to glucose. \* or \*\* $P=0.0079$ ,  $P=0.0197$ ,  $P=0.0343$  and  $P=0.0207$ , from left to right. **h**, Insulin levels at 0 min and 15 min after glucose load. **i**, Serum ALT. **j**, Serum AST. **k**, Serum triglyceride. **l**, Serum total cholesterol. **m**, Hepatic triglyceride. **n**, Hepatic total cholesterol. In **a–n**,  $n=6$ . **o**, Representative H&E and ORO staining of liver sections ( $n=4$  mice per group, three images per mouse per staining). Scale bar, 100 μm. **p**, Left, representative BrdU staining of intestine sections ( $n=5$  mice per group, nine images per mouse). Scale bars, 100 μm. Right, BrdU labelling index;  $n=5$ . **q**, ChREBP and CERS4 protein levels in the intestine. **r**, *Myc* and *Gcg* mRNA levels in the intestine;  $n=6$ . **s,t**, Total GLP-1 (**s**) and active GLP-1 levels (**t**) in the portal vein blood;  $n=6$ . **u**, *Cers4* mRNA levels in the intestine;  $n=6$ . **v**, Serum ceramide levels;  $n=6$ . **w–y**, Hepatic expression of genes involved in lipid synthesis, transport and beta-oxidation (**w**), glycolysis (**x**) and gluconeogenesis (**y**);  $n=6$ , \* or \*\* or \*\*\* $P=0.0235$ ,  $P=0.0255$ ,  $P=0.0295$ ,  $P=0.0289$ ,  $P=0.0052$ ,  $P=0.0381$ ,  $P=0.0063$ ,  $P=0.0496$ ,  $P=0.0035$ ,  $P=0.0022$ ,  $P=0.0004$ ,  $P=0.0097$ ,  $P=0.0007$ ,  $P=0.0090$ ,  $P=0.0353$ ,  $P<0.0001$ ,  $P=0.0013$ ,  $P=0.0262$ ,  $P=0.0026$ ,  $P=0.0019$ ,  $P=0.0011$ ,  $P<0.0001$ ,  $P=0.0013$ ,  $P=0.0087$ ,  $P=0.0378$  and  $P=0.0437$ , from left to right. All data are presented as the mean ± s.e.m. of biologically independent samples, analysed using a two-tailed Student's t-test (**a–g, i–n, p** and **r–y**) or two-tailed paired t-test (**h**).

studies of the effect of intravenous GLP-1 infusion on appetite regulation found that increasing the GLP-1 dose at a high rate exerted greater inhibition on energy intake than at a low rate of infusion.

Indeed, a weak effect on appetite was found at the more ‘physiological’ levels of GLP-1 (ref. 45). In the current study, the increase in portal GLP-1 levels might not be high enough to reduce food intake.



Future studies using GLP-1 shRNA or knock-down mice are warranted for further exploration of whether intestinal *Myc* disruption improves HFD-induced metabolic disorders through GLP-1.

Another interesting pathway implicated by the RNA-seq analysis is the sphingolipid metabolism. Ceramide is the central constituent of sphingolipids and an exciting class of bioactive lipids that

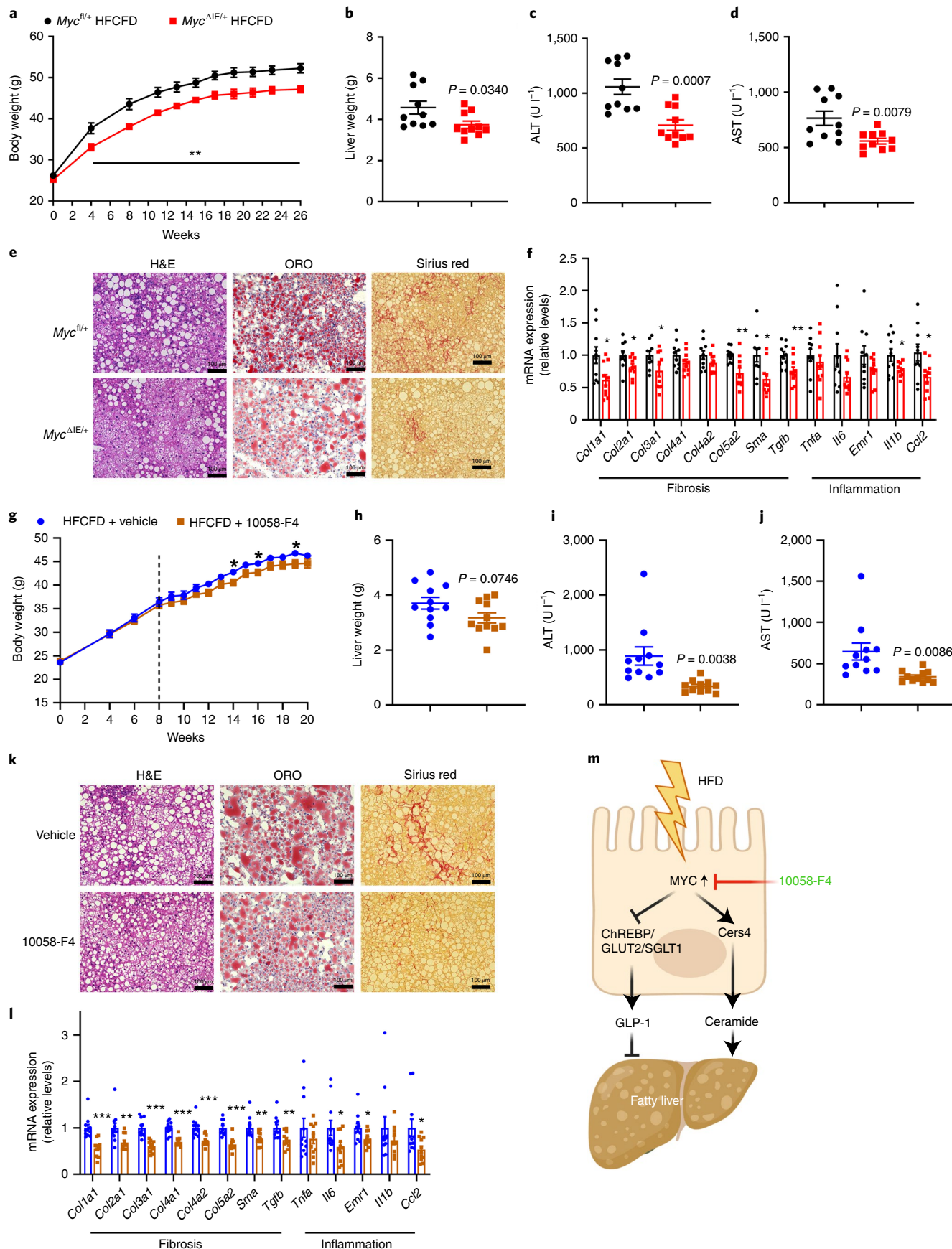


**Fig. 8 | Inhibition of MYC in the intestine improved HFCFD-induced liver fibrosis.** **a–f**, *Myc<sup>fl/fl</sup>* and *Myc<sup>ΔIE/+</sup>* mice were fed a HFCFD for 26 weeks. Data are representative of  $n=2$  experiments. **a**, Body weight curve.  $**P=0.0081$  for 4 weeks,  $P=0.0020$  for 8 weeks,  $P=0.0016$  for 11 weeks,  $P=0.0042$  for 13 weeks,  $P=0.0041$  for 15 weeks,  $P=0.0022$  for 17 weeks,  $P=0.0050$  for 19 weeks,  $P=0.0045$  for 21 weeks,  $P=0.0023$  for 23 weeks and  $P=0.0015$  for 26 weeks. **b**, Liver weight. **c**, Serum ALT. **d**, Serum AST. In **a–d**,  $n=10$ . **e**, Representative H&E and ORO and Sirius red staining of liver sections ( $n=4$  mice per group, three images per mouse per staining). Scale bar, 100  $\mu\text{m}$ . **f**, Hepatic expression of genes involved in fibrosis and inflammation;  $n=10$ . \* or  $**P=0.0220$ ,  $P=0.0357$ ,  $P=0.0415$ ,  $P=0.0043$ ,  $P=0.0126$ ,  $P=0.0096$ ,  $P=0.0472$  and  $P=0.0246$ , from left to right. **g–l**, C57BL/6N mice were first fed a HFCFD for 8 weeks and then gavaged daily with vehicle or 50 mg per kg (body weight) 10058-F4 while maintained on HFCFD for another 12 weeks. Data are representative of  $n=2$  experiments. **g**, Body weight curve.  $*P=0.0227$  for 14 weeks,  $P=0.0422$  for 16 weeks and  $P=0.0366$  for 19 weeks. **h**, Liver weight. **i**, Serum ALT. **j**, Serum AST. **g–j**,  $n=11$ . **k**, Representative H&E and Oil Red O and Sirius red staining of liver sections ( $n=4$  mice per group, three images per mouse per staining). Scale bar, 100  $\mu\text{m}$ . **l**, Hepatic expression of genes involved in fibrosis and inflammation;  $n=11$ . \* or \*\* or \*\*\* $P<0.0001$ ,  $P=0.0094$ ,  $P<0.0001$ ,  $P=0.0005$ ,  $P<0.0001$ ,  $P=0.0091$ ,  $P=0.0077$ ,  $P=0.0393$ ,  $P=0.0298$  and  $P=0.0311$ , from left to right. All data are presented as the mean  $\pm$  s.e.m. of biologically independent samples, analysed using a two-tailed Student's *t*-test (**a–d**, **f**, **g–j** and **l**). **m**, Schematic depicting the intestinal MYC-GLP-1 and MYC-ceramide regulatory axes that underly fatty liver disease. Created with BioRender.com.

has attracted great attention in the regulation of metabolic diseases. Ceramides were proposed as the 21st century cholesterol<sup>46</sup>, with markedly elevated levels in the serum of patients with NAFLD<sup>47</sup>, atherosclerosis<sup>48,49</sup> and T2DM<sup>50,51</sup>. Notably, ceramide levels positively correlate with the severity of insulin resistance<sup>51</sup> and hepatic lipid accumulation<sup>21,52</sup>. Administration of ceramides to mice aggravates virtually all metabolic disorders<sup>53–56</sup>. A causal role of ceramides in promoting metabolic disorders was demonstrated by pharmacological or genetical manipulation of ceramide biosynthesis and catabolism in rodent models<sup>55–58</sup>. The current study showed that mice with reduced MYC expression in the intestine were resistant to diet-induced metabolic disorders, and this resistance was correlated with lower serum ceramides. Exogenously administered ceramide C16:0 increased different ceramide species in the serum and abrogated the improvement in obesity, insulin resistance and hepatic steatosis in *Myc<sup>ΔIE/+</sup>* mice as compared to *Myc<sup>fl/fl</sup>* mice, suggesting that ceramides could dynamically interconvert into other species in vivo and at least partially mediate the metabolic improvements by intestinal MYC disruption. However, whether the intestinal MYC-GLP-1 pathway and the intestinal MYC-ceramide pathway interact with each other, and whether mechanisms other than GLP-1 and ceramides contribute to the beneficial metabolic effects are unknown and await further study. Besides, the roles of colonic MYC and intestinal cell-type-specific MYC in metabolic diseases are worth investigating in the future.

Ceramide synthases (CERS) catalyse *N*-acylation of (dihydro-) sphingosine to (dihydro-) ceramide, consisting of six members (CERS1–6) with different substrate specificities and expression patterns. With the effect of ceramides on physiological and pathophysiological processes being extensively studied, the precise mechanism underlying CERS regulation is largely unknown<sup>59</sup>. Here, a new mechanism was uncovered in which *Cers4* was specifically regulated by MYC in the intestine, as a target gene among all the CERS family genes. With *Cers4* preferentially synthesizing C18-Cer to C24-Cer<sup>60–62</sup>, there are two possible explanations for the decrease of C16-Cer to C24-Cer observed with intestinal *Myc* disruption: (1) in addition to *Cers4*, intestinal MYC regulated the expression of SMPD3 in the sphingomyelinase pathway, although the detailed mechanism awaits future investigation, and (2) the possibility exists that ceramides could interconvert into other species in vivo.

Great efforts have been invested into the discovery of MYC inhibitors because of its profound functions, especially for cancer therapy<sup>63</sup>. Here, 10058-F4, a MYC-MAX interaction inhibitor, was orally administered to obese mice and improved obesity, insulin resistance, hepatic steatosis and fibrosis. The compound 10058-F4 undergoes fast clearance with a measured in vivo half-life of about 1 h, leading to low concentrations in tissues and failure of the anti-tumour activity<sup>64</sup>. The levels of MYC inhibition to be achieved to confer metabolic improvements should be much lower than the levels to confer anti-tumour effects, with the latter mainly

dependent on the anti-proliferative effect of MYC inhibitors. In the current study, neither genetic reduction of *Myc* nor 10058-F4 treatment, at least at the dose used here, affected intestinal cell proliferation. Instead, the metabolic benefits were mediated through changes in GLP-1 and ceramides. Because there is currently no therapy for NASH, the intestinal MYC pathway may be a new area of investigation to treat this disorder.

In conclusion, this study delineates a previously undefined role of intestinal MYC in metabolic diseases via regulation of GLP-1 and ceramides. Genetic reduction or pharmacological inhibition of intestinal MYC protects against diet-induced obesity, NAFLD and NASH, highlighting intestinal MYC as a potential target for treating metabolic disorders.

## Methods

**Mouse studies.** *Myc<sup>fl/fl</sup>* mice were provided by J. M. Sedivy (Brown University) and described previously<sup>6,65</sup>. Villin-cre and villin-ERT2-cre mice were provided by D. L. Gumucio (University of Michigan) and P. Chambon (GBMC, Illkirch, France), respectively, and described previously<sup>66,67</sup>. All mouse strains are on the C57BL/6 genetic background. For intestine-specific disruption, villin-cre *Myc<sup>fl/fl</sup>* (*Myc<sup>ΔIE</sup>*) and villin-cre *Myc<sup>ΔIE/+</sup>* (*Myc<sup>ΔIE/+</sup>*) mice were generated by crossing *Myc<sup>fl/fl</sup>* mice with the villin-cre mice. For temporal intestine-specific disruption, villin-ERT2-cre *Myc<sup>fl/fl</sup>* (*Myc<sup>ΔIEERT2</sup>*) mice were generated by crossing the *Myc<sup>fl/fl</sup>* mice with the villin-ERT2-cre mice. To activate the ERT2-cre, mice were injected intraperitoneally with 100 mg per kg (body weight) tamoxifen (Sigma) on 3 consecutive days and received 100 mg per kg (body weight) tamoxifen injection weekly until the end of the studies. HFD (60 kcal% from fat) was purchased from Bio-Serv. HFCFD with 40 kcal% from fat (mostly palm oil), 20 kcal% from fructose and 2 kcal% from cholesterol was purchased from Research Diets (D09100310). Male littermates 7- to 8-weeks old were fed a chow diet or HFD or HFCFD for the indicated time to induce obesity, hepatic steatosis and fibrosis. For the ceramide turnover study, C16:0 ceramide, purchased from Avanti Polar Lipids, was suspended in saline with 0.5% sodium carboxymethyl cellulose and 2% Tween 80. Male *Myc<sup>fl/fl</sup>* and *Myc<sup>ΔIE/+</sup>* mice 7- to 8-weeks old were fed on a HFD and injected intraperitoneally every day with vehicle or 10 mg per kg (body weight) C16:0 ceramide for 6 weeks. For the MYC inhibitor studies, 10058-F4, purchased from MedChem Express, was suspended in saline with 0.5% sodium carboxymethyl cellulose, 2.5% Tween 80 and 2.5% DMSO. For the obesity and steatosis model, male C57BL/6N mice 7- to 8-weeks old were first fed a HFD for 6 weeks and then administered with vehicle or 50 mg per kg (body weight) 10058-F4 by gavage daily while they were maintained on a HFD for another 8 weeks. To check dependency on intestinal MYC, 7- to 8-week-old male *Myc<sup>fl/fl</sup>* and *Myc<sup>ΔIE/+</sup>* mice were fed a HFD and administered with vehicle or 50 mg per kg (body weight) 10058-F4 by gavage daily for 8 weeks. For the NASH model, 7- to 8-week-old male C57BL/6N mice were first fed a HFCFD for 8 weeks and then administered with vehicle or 50 mg per kg (body weight) 10058-F4 by gavage daily while they were maintained on HFCFD for another 12 weeks. Mice were maintained in a temperature-controlled room at 20–24 °C and average humidity at 40% under a standard 12-h light/12-h dark cycle with water and food provided ad libitum. All mouse studies were approved by the National Cancer Institute Animal Care and Use Committee and performed in accordance with the Institute of Laboratory Animal Resources guidelines.

**Human cohort.** Mucosal biopsy samples of the distal ileum were taken from individuals who were not diagnosed with inflammatory bowel disease or colorectal cancer during routine colonoscopy. The sexes and ages were at similar levels in the obese group (BMI  $\geq 25$ ;  $n=16$ ) and non-obese group (BMI  $< 25$ ;  $n=28$ ), with clinical variables listed in Supplementary Table 2. All individuals met the following

inclusion criteria: (1) no inflammatory bowel disease; (2) no colorectal cancer; (3) no colorectal polyps; (4) no acute or chronic viral hepatitis; (5) no pregnancy; (6) no alcoholic liver disease or daily drinking habits; and (7) no disease judged by clinicians as unsuitable for biopsy. The study has been approved by the Ethics Committee of Shanghai Tenth People's Hospital, and all individuals gave written informed consent before participating in the study. The biopsies were used for real-time PCR analysis.

**Quantitative real-time PCR.** Total RNA was extracted using TRIzol (Invitrogen). cDNA was synthesized from 1 µg total RNA using qScript cDNA SuperMix. Real-time PCR primer sequences are included in Supplementary Table 3. The relative amount of each mRNA was calculated after normalizing to their corresponding *Actb* or *Gapdh* mRNA, and the results were expressed as fold change values relative to the control group values.

**Western blotting.** Tissues or cultured organoids were lysed with RIPA lysis buffer with protease inhibitors. Protein concentrations were determined by the BCA protein assay kit (Pierce Chemical). The samples were subjected to SDS-PAGE, transferred to polyvinylfluoride membranes, and incubated overnight at 4°C with antibodies against MYC (Santa Cruz, sc-41), ChREBP (Abcam, ab92809), CERS4 (Abcam, ab66512), SMPD3 (Santa Cruz, sc-166637), cleaved NOTCH1 (Cell Signaling Technology, 4147), RBP-J (Cell Signaling Technology, 5313), ATOH1 (Proteintech, 21215-1-AP), HES1 (Santa Cruz, sc-166410) and ACTB (Cell Signaling Technology, 4970). Proteins were visualized using the SuperSignal West Dura Extended Duration Substrate (Thermo Fisher Scientific) and an image analyser (Alpha Innotech).

**Metabolic assays.** For the GTT, mice were fasted overnight for 16 h. For the ITT, mice were fasted for 4 h. Glucose (2 grams per kg body weight for chow-fed mice alone, 1.5 grams per kg body weight for HFD-fed mice alone and 1.8 grams per kg body weight when chow-fed mice and HFD-fed mice were measured together) or insulin (Eli Lilly; 0.8 U kg<sup>-1</sup> for chow-fed mice alone, 0.9 U kg<sup>-1</sup> for HFD-fed mice alone and 0.85 U kg<sup>-1</sup> when chow-fed mice and HFD-fed mice were measured together) in saline was injected intraperitoneally to conscious animals, and blood glucose was measured from the tail vein before and at 15, 30, 60 and 90 min after injection by using a glucometer (Bayer).

**Histological analysis.** Formalin-fixed paraffin-embedded liver and intestine sections were stained by H&E or Sirius red or Alcian blue and OCT-embedded frozen liver sections were stained by ORO according to standard protocols followed by microscopic examination.

**Bromodeoxyuridine staining.** To assess cell proliferation in the intestine, mice were intraperitoneally injected with 20 mg per kg body weight BrdU (Sigma). Two hours later, the mice were killed by CO<sub>2</sub> asphyxiation, and the intestine dissected and fixed in 10% PBS-buffered formalin before embedding in paraffin. BrdU immunostaining was carried out using a BrdU Detection Kit (BD Biosciences). The BrdU labelling index was determined by calculating the percentage of BrdU-positive nuclei in nine random ×40 microscopic fields per mouse.

**Immunohistochemistry staining.** Immunohistochemistry staining was performed on formalin-fixed paraffin-embedded intestine and subcutaneous white adipose tissue sections. After overnight incubation with anti-MYC antibody (Abcam, ab39688), anti-lysozyme antibody (Dako, EC3.2.1.17), anti-synaptophysin (Thermo Fisher Scientific, MA5-14532) or anti-UCP-1 antibody (Abcam, ab10983), the slides were incubated for 1 h with horseradish peroxidase-conjugated secondary antibodies. The intensity of indicated proteins was detected using the DAB kit (Vector Laboratories).

**In situ hybridization.** In situ hybridization was performed with RNAscope Probe-Mm-Myc (Advanced Cell Diagnostics, 413451) using RNAscope 2.5 HD Detection Reagents-RED kit (Advanced Cell Diagnostics, 322360) following the manufacturer's instruction.

**Lipid analysis.** Hepatic and serum triglyceride and cholesterol and non-esterified fatty acid levels were determined with assay kits from Wako Diagnostics (Wako Chemicals) following the manufacturer's instructions. To measure faecal lipids, mice were housed individually in separate cages, and faeces were collected during a 48-h period and dried. Dried faeces were weighed and extracted with chloroform:methanol (2:1) solution and dissolved in PBS containing 1% Triton X-100 after evaporation. Triglyceride and cholesterol and non-esterified fatty acid levels were determined with assay kits from Wako Diagnostics (Wako Chemicals) following the manufacturer's instructions.

**Serum aminotransferase assay.** ALT and AST levels were assessed in a 96-well microplate using commercial ALT and AST assay kits (Catachem) and monitored at 340 nm for 15 min with a microplate reader (BioAssay Systems).

**Serum insulin assay.** Serum insulin levels were measured with a mouse insulin ELISA kit (Crystal Chem) following the manufacturer's protocol.

**Lipidomics analysis.** Serum global lipidomics was performed as previously described<sup>55</sup>. Briefly, 50 µl of serum was extracted with 200 µl of a chloroform:methanol (2:1) solution. After vortex and centrifuge, the lower organic phase was collected and evaporated. For serum global lipidomics, the multivariate data matrix was analysed by SIMCA-P+ 15 software (Umetrics). For ceramide quantification, the data were analysed by TargetLynx software, a subroutine of the MassLynx v4.2 software (Waters). The ceramide standards, including C16:0, C18:0, C18:1, C20:0, C22:0, C24:0 and C24:1, were obtained from Avanti Polar Lipids.

For quantification of ceramides in intestinal organoids and culture medium, intestinal organoids were homogenized with 250 µl deionized water. A total of 200 µl of the homogenized organoids or 200 µl of the culture medium was extracted with 800 µl of a chloroform:methanol (2:1) solution and then processed the same as for serum lipidomics. The remaining homogenized organoids were used to measure protein concentration by the BCA protein assay kit (Pierce Chemical). Ceramide levels of intestinal organoids and culture medium were normalized to the total protein content of the organoids.

**Body composition and indirect calorimetry.** Body fat and lean mass of non-anaesthetized live mice were determined using an EchoMRI 3-in-1 mouse scanner, following the manufacturer's protocol. Indirect calorimetry was carried out on 4-week HFD-fed *Myc*<sup>ΔIE/+</sup> and *Myc*<sup>ΔIE/ΔIE</sup> mice using a 12-chamber Environment Controlled CLAMS (Columbus Instruments) with one mouse in each chamber as previously described<sup>55</sup>. Mice were tested every 13 min for 3 d at 22°C and 1 d at 30°C. Temperature was changed on day 4 at 6:00. During testing, food and water were provided ad libitum. Twenty-four-hour-average parameters were analysed from data collected at day 3 for 22°C, and day 4 for 30°C (excluding the first hour after temperature changes).

**Luciferase reporter assay.** MYC binding sequences, known as Ebox sequences, are predicted by the Genomatix MatInspector. Custom GeneBlocks containing the predicted Ebox sites in the promoter region of mouse *Cers4* and *Smpd3* were synthesized by IDT DNA Technologies and cloned into the pGL4.11 luciferase vector (Promega). Mouse colon cancer cell line MC38 cells were seeded into a 12-well plate and cultured in DMEM supplemented with 10% FBS and 1% antibiotic. Ebox reporter vectors and phRL-TK *Renilla* luciferase control vector (Promega) were co-transfected into MC38 cells by use of Lipofectamine 3000 transfection reagent (Thermo Fisher Scientific). In addition, either a MYC expression vector pCX-Myc<sup>ΔS</sup> (Addgene, 19772) or the empty backbone vector was co-transfected into the cells and a final concentration of 40 µM 10058-F4 or DMSO was added to the culture medium to inhibit MYC activity. Empty vector (pGL4.11) was used as a negative control. At 36 h after the transfection, luciferase assays were performed by use of the dual-luciferase assay system (Promega). Firefly and *Renilla* luciferase activities were measured by Veritas microplate luminometer (Turner Biosystems).

**Chromatin immunoprecipitation assay.** ChIP for MYC binding was performed in accordance with the manufacturer's protocol of ChIP-IT High Sensitivity Kit (Active Motif). Chromatin was prepared from isolated nuclei of formaldehyde cross-linked MC38 cells and sheared to between 200 and 500 bp. Sheared chromatin was immunoprecipitated with anti-MYC antibody (Cell Signaling Technology, 9402), or anti-pan-H3 antibody (Cell Signaling Technology, 4620) or normal rabbit IgG (Cell Signaling Technology, 2729). The precipitated DNA samples were incubated with RNase A and proteinase K, purified using MinElute Reaction Cleanup Kit (QIAGEN) and subjected to real-time PCR using primers listed in Supplementary Table 3. Threshold cycle (Ct) values of ChIP and input samples were calculated and presented as fold change values.

**Intestinal organoid isolation and treatment.** Intestines were removed from *Myc*<sup>ΔIE/+</sup> and *Myc*<sup>ΔIE/ΔIE</sup> mice fed a HFD for 2 weeks and opened longitudinally and washed with ice-cold PBS. Crypts and villi were exposed by dicing the intestines into small pieces (around 2 mm), followed by extensive washes to remove contaminants. Then, Gentle Cell Dissociation Reagent (Stemcell Technologies, 7174) was used according to the manufacturer's instruction. Briefly, intestinal pieces were incubated on a gently rotating platform for 15 min. Subsequently, the dissociation reagent was removed and intestinal pieces were washed with PBS containing 0.1% BSA by vigorous pipetting. The washing step was repeated four times, and the supernatant was collected from each wash and labelled as fractions 1–4. The first and second fractions that usually contain loose pieces of mesenchyme and villi were not used. Fractions three and four containing the intestinal crypts were pooled and filtered through a 70-µm nylon cell strainer (Corning, 352350). Crypts were counted, then embedded in Matrigel (Corning, 354230) and cultured in IntestiCult Organoid Growth Medium (Stemcell Technologies, 6005). Medium was changed every 2 or 3 d. On day 6, the intestinal organoids were treated with vehicle, 20 µM or 40 µM 10058-F4 (MedChem Express), 10 µM KJ-Pyr-9 (Sigma), control BSA or BSA-conjugated FA (0.2 mM palmitic acid + 0.4 mM oleic acid; Sigma, 76119 and O1383). Intestinal organoids were collected 24 h after treatment for RNA analysis, and 48 h after treatment for protein analysis. Both organoids and culture medium were collected 48 h after treatment for ceramide analysis.

For lentiviral transduction experiments, organoids were collected and placed in 15 ml Corning tubes. The supernatant was removed by centrifugation and

we added control lentiviruses or lentiviruses carrying *Cers4* shRNA or *Cers4* overexpression cDNA (purchased from VectorBuilder, sequence available upon request) at 10<sup>6</sup> plaque-forming units per 100 crypts. The organoid-virus mixture was placed in an incubator at 37 °C for 1 h. Then, 500 µl culture medium was added to the organoid-virus mixture followed by centrifugation to discard the supernatant. Finally, organoids were embedded in Matrigel and cultured as described above. Organoids and culture medium were collected 6 d later for RNA, protein and ceramide analysis.

**GLP-1 secretion assay.** For in vivo GLP-1 secretion, mice were fasted for 6 h, gavaged with 25 mg per kg (body weight) sitagliptin (Sigma) 1 h before a glucose bolus (2 g per kg body weight). Fifteen minutes after glucose gavage, mice were killed by CO<sub>2</sub> asphyxiation and portal vein blood or peripheral blood was collected. Serum GLP-1 was measured as described below.

For in vitro GLP-1 secretion, intestinal organoids were isolated from *Myc*<sup>dfl/+</sup> and *Myc*<sup>Δf/f</sup> mice fed a HFD for 2 weeks and cultured for 7 d. On day 7, after 30 min glucose deprivation in DMEM no-glucose medium, a 1-h GLP-1 secretion test in response to DMEM without glucose and to DMEM with glucose (5.5 mmol l<sup>-1</sup>) was performed at 37 °C in DMEM plus 1% dipeptidyl peptidase-IV inhibitor (Millipore). Finally, the medium was collected and centrifuged for 5 min at 4 °C at 13,000g. For the MYC inhibitor experiment, organoids were pretreated with DMSO or 40 µM 10058-F4 24 h before the GLP-1 secretion test. Medium GLP-1 was measured as described below. The protein content of the remaining organoids was assessed by the BCA protein assay kit (Pierce Chemical).

Total GLP-1 and active GLP-1 were measured by ELISA kits EZGLP1T-36K and EGLP-35K (Millipore), respectively. Medium GLP-1 levels were normalized to the total quantity of cellular protein.

**RNA-seq library preparation and data analysis.** Total RNA was isolated from mouse intestines using RNeasy Plus Mini Kit (Qiagen, 74136) according to the manufacturer's instructions. RNA-seq libraries were prepared using Illumina TruSeq Stranded mRNA Library Prep (Illumina). Samples were pooled and sequenced on a HiSeq 4000 (Illumina) using a paired-end protocol.

For RNA-seq data analysis, reads of the samples were trimmed for adaptors and low-quality bases using Trimmomatic 0.36 software before alignment with the mouse reference genome (mm10) and the annotated transcripts using STAR 2.5.1. The mapping statistics were calculated using Picard 1.84 software. Library complexity was measured in terms of unique fragments in the mapped reads using Picard's MarkDuplicate utility. The gene expression quantification analysis was performed for all samples using STAR/RSEM 1.2.22 tools. Differential gene expression was assessed with DESeq2 using the parameters: adjusted *P* value of 0.05 and log<sub>2</sub> fold change of 0.585 (for 1.5-fold differentially expressed genes). Functional enrichment analysis was performed with DAVID<sup>69,70</sup> using the pathways related to metabolism from the KEGG database annotation.

**Statistics and reproducibility.** All data were replicated in at least two independent experiments, except for the RNA-seq analysis and data generated with human ileum biopsies, and sample sizes for reproducibility are indicated in the figure legends. Statistical analysis was performed using Prism version 8.4.3 (GraphPad software). No statistical tool was used to predetermine sample sizes; rather, the availability of materials and estimates of variances based on previous experience determined the number of biological replicates that were used. Experimental values are presented as the mean ± s.e.m. Statistical significance between two groups was determined using a two-tailed Student's *t*-test. For comparing insulin levels at 15 min with those at 0 min, a two-tailed paired *t*-test was performed. One-way ANOVA followed by Tukey's multiple-comparisons test or two-way ANOVA followed by Tukey's or Dunnett's multiple-comparisons test was applied for multi-group comparisons, as indicated in the figure legends. Correlations were assessed by non-parametric Spearman's test. *P* values were calculated with confidence intervals of 95%, and differences were considered statistically significant at *P* < 0.05. Exact *P* values are indicated in the figures and corresponding figure legends, except for *P* < 0.0001.

**Reporting Summary.** Further information on research design is available in the Nature Research Reporting Summary linked to this article.

## Data availability

Transcriptomic data have been deposited in the Gene Expression Omnibus under accession code GSE155460. Source data are provided with this paper.

Received: 26 August 2020; Accepted: 26 May 2021;  
Published online: 1 July 2021

## References

- Ray, K. NAFLD—the next global epidemic. *Nat. Rev. Gastroenterol. Hepatol.* **10**, 621 (2013).
- Younossi, Z. et al. Global burden of NAFLD and NASH: trends, predictions, risk factors and prevention. *Nat. Rev. Gastroenterol. Hepatol.* **15**, 11–20 (2018).
- Anstee, Q. M., Targher, G. & Day, C. P. Progression of NAFLD to diabetes mellitus, cardiovascular disease or cirrhosis. *Nat. Rev. Gastroenterol. Hepatol.* **10**, 330–344 (2013).
- Wong, R. J., Cheung, R. & Ahmed, A. Non-alcoholic steatohepatitis is the most rapidly growing indication for liver transplantation in patients with hepatocellular carcinoma in the U.S. *Hepatology* **59**, 2188–2195 (2014).
- Friedman, S. L., Neuschwander-Tetri, B. A., Rinella, M. & Sanyal, A. J. Mechanisms of NAFLD development and therapeutic strategies. *Nat. Med.* **24**, 908–922 (2018).
- Meyer, N. & Penn, L. Z. Reflecting on 25 years with MYC. *Nat. Rev. Cancer* **8**, 976–990 (2008).
- Dang, C. V. MYC on the path to cancer. *Cell* **149**, 22–35 (2012).
- Qu, A. et al. Role of Myc in hepatocellular proliferation and hepatocarcinogenesis. *J. Hepatol.* **60**, 331–338 (2014).
- Shachaf, C. M. et al. MYC inactivation uncovers pluripotent differentiation and tumour dormancy in hepatocellular cancer. *Nature* **431**, 1112–1117 (2004).
- Shroff, E. H. et al. MYC oncogene overexpression drives renal cell carcinoma in a mouse model through glutamine metabolism. *Proc. Natl Acad. Sci. USA* **112**, 6539–6544 (2015).
- Osthuis, R. C. et al. Dereulation of glucose transporter 1 and glycolytic gene expression by c-Myc. *J. Biol. Chem.* **275**, 21797–21800 (2000).
- Peterson, C. W. & Ayer, D. E. An extended Myc network contributes to glucose homeostasis in cancer and diabetes. *Front. Biosci.* **16**, 2206–2223 (2011).
- Nevzorova, Y. A. et al. Enhanced expression of c-myc in hepatocytes promotes initiation and progression of alcoholic liver disease. *J. Hepatol.* **64**, 628–640 (2016).
- Shin, J. et al. SIRT7 represses myc activity to suppress ER stress and prevent fatty liver disease. *Cell Rep.* **5**, 654–665 (2013).
- Gouw, A. M. et al. The MYC oncogene cooperates with sterol-regulated element-binding protein to regulate lipogenesis essential for neoplastic growth. *Cell Metab.* **30**, 556–572 e555 (2019).
- Davis, A. C., Wims, M., Spotts, G. D., Hann, S. R. & Bradley, A. A null c-myc mutation causes lethality before 10.5 days of gestation in homozygotes and reduced fertility in heterozygous female mice. *Genes Dev.* **7**, 671–682 (1993).
- Hofmann, J. W. et al. Reduced expression of MYC increases longevity and enhances health span. *Cell* **160**, 477–488 (2015).
- Gonzalez, F. J., Jiang, C. & Patterson, A. D. An intestinal microbiota-farnesoid X receptor axis modulates metabolic disease. *Gastroenterology* **151**, 845–859 (2016).
- Gonzalez, F. J., Xie, C. & Jiang, C. The role of hypoxia-inducible factors in metabolic diseases. *Nat. Rev. Endocrinol.* **15**, 21–32 (2018).
- Chaurasia, B. & Summers, S. A. Ceramides—lipotoxic inducers of metabolic disorders. *Trends Endocrinol. Metab.* **26**, 538–550 (2015).
- Pagadala, M., Kasumov, T., McCullough, A. J., Zein, N. N. & Kirwan, J. P. Role of ceramides in non-alcoholic fatty liver disease. *Trends Endocrinol. Metab.* **23**, 365–371 (2012).
- Samuel, V. T. & Shulman, G. I. Mechanisms for insulin resistance: common threads and missing links. *Cell* **148**, 852–871 (2012).
- Summers, S. A., Chaurasia, B. & Holland, W. L. Metabolic Messengers: ceramides. *Nat. Metab.* **1**, 1051–1058 (2019).
- Hannun, Y. A. & Obeid, L. M. Sphingolipids and their metabolism in physiology and disease. *Nat. Rev. Mol. Cell Biol.* **19**, 175–191 (2018).
- Liang, S. J., Li, X. G. & Wang, X. Q. Notch signaling in mammalian intestinal stem cells: determining cell fate and maintaining homeostasis. *Curr. Stem Cell Res. Ther.* **14**, 583–590 (2019).
- Sancho, R., Cremona, C. A. & Behrens, A. Stem cell and progenitor fate in the mammalian intestine: Notch and lateral inhibition in homeostasis and disease. *EMBO Rep.* **16**, 571–581 (2015).
- Andersen, A., Lund, A., Knop, F. K. & Vilksboll, T. Glucagon-like peptide 1 in health and disease. *Nat. Rev. Endocrinol.* **14**, 390–403 (2018).
- Gorbolev, V. et al. Na<sup>+</sup>-D-glucose cotransporter SGLT1 is pivotal for intestinal glucose absorption and glucose-dependent incretin secretion. *Diabetes* **61**, 187–196 (2012).
- Gribble, F. M., Williams, L., Simpson, A. K. & Reimann, F. A novel glucose-sensing mechanism contributing to glucagon-like peptide-1 secretion from the GLUTag cell line. *Diabetes* **52**, 1147–1154 (2003).
- Kuhre, R. E., Frost, C. R., Svendsen, B. & Holst, J. J. Molecular mechanisms of glucose-stimulated GLP-1 secretion from perfused rat small intestine. *Diabetes* **64**, 370–382 (2015).
- Parker, H. E. et al. Predominant role of active versus facilitative glucose transport for glucagon-like peptide-1 secretion. *Diabetologia* **55**, 2445–2455 (2012).
- Reimann, F. et al. Glucose sensing in L cells: a primary cell study. *Cell Metab.* **8**, 532–539 (2008).
- Filhoulaud, G., Guilmeau, S., Dentin, R., Girard, J. & Postic, C. Novel insights into ChREBP regulation and function. *Trends Endocrinol. Metab.* **24**, 257–268 (2013).

34. Trabelsi, M. S. et al. Farnesoid X receptor inhibits glucagon-like peptide-1 production by enteroendocrine L cells. *Nat. Commun.* **6**, 7629 (2015).
35. Mao, J. et al. Overnutrition stimulates intestinal epithelium proliferation through beta-catenin signaling in obese mice. *Diabetes* **62**, 3736–3746 (2013).
36. Petit, V. et al. Chronic high-fat diet affects intestinal fat absorption and postprandial triglyceride levels in the mouse. *J. Lipid Res.* **48**, 278–287 (2007).
37. Beyaz, S. et al. High-fat diet enhances stemness and tumorigenicity of intestinal progenitors. *Nature* **531**, 53–58 (2016).
38. He, T. C. et al. Identification of c-MYC as a target of the APC pathway. *Science* **281**, 1509–1512 (1998).
39. Bettess, M. D. et al. c-Myc is required for the formation of intestinal crypts but dispensable for homeostasis of the adult intestinal epithelium. *Mol. Cell. Biol.* **25**, 7868–7878 (2005).
40. Cho, Y. M., Fujita, Y. & Kieffer, T. J. Glucagon-like peptide-1: glucose homeostasis and beyond. *Annu. Rev. Physiol.* **76**, 535–559 (2014).
41. Nauck, M. A. et al. Normalization of fasting hyperglycaemia by exogenous glucagon-like peptide 1 (7-36 amide) in type 2 (non-insulin-dependent) diabetic patients. *Diabetologia* **36**, 741–744 (1993).
42. Rachman, J., Barrow, B. A., Levy, J. C. & Turner, R. C. Near-normalisation of diurnal glucose concentrations by continuous administration of glucagon-like peptide-1 (GLP-1) in subjects with NIDDM. *Diabetologia* **40**, 205–211 (1997).
43. Holst, J. J. The physiology of glucagon-like peptide 1. *Physiol. Rev.* **87**, 1409–1439 (2007).
44. Tang-Christensen, M., Vrang, N. & Larsen, P. J. Glucagon-like peptide 1 (7-36) amide's central inhibition of feeding and peripheral inhibition of drinking are abolished by neonatal monosodium glutamate treatment. *Diabetes* **47**, 530–537 (1998).
45. Verdich, C. et al. A meta-analysis of the effect of glucagon-like peptide-1 (7-36) amide on ad libitum energy intake in humans. *J. Clin. Endocrinol. Metab.* **86**, 4382–4389 (2001).
46. Summers, S. A. Could ceramides become the new cholesterol? *Cell Metab.* **27**, 276–280 (2018).
47. Gorden, D. L. et al. Biomarkers of NAFLD progression: a lipidomics approach to an epidemic. *J. Lipid Res.* **56**, 722–736 (2015).
48. Laaksonen, R. et al. Plasma ceramides predict cardiovascular death in patients with stable coronary artery disease and acute coronary syndromes beyond LDL cholesterol. *Eur. Heart J.* **37**, 1967–1976 (2016).
49. Vorkas, P. A. et al. Metabolic phenotyping of atherosclerotic plaques reveals latent associations between free cholesterol and ceramide metabolism in atherogenesis. *J. Proteome Res.* **14**, 1389–1399 (2015).
50. Chavez, J. A. & Summers, S. A. A ceramide-centric view of insulin resistance. *Cell Metab.* **15**, 585–594 (2012).
51. Haus, J. M. et al. Plasma ceramides are elevated in obese subjects with type 2 diabetes and correlate with the severity of insulin resistance. *Diabetes* **58**, 337–343 (2009).
52. Yetukuri, L. et al. Bioinformatics strategies for lipidomics analysis: characterization of obesity-related hepatic steatosis. *BMC Syst. Biol.* **1**, 12 (2007).
53. Jiang, C. et al. Intestinal farnesoid X receptor signaling promotes non-alcoholic fatty liver disease. *J. Clin. Invest.* **125**, 386–402 (2015).
54. Jiang, C. et al. Intestine-selective farnesoid X receptor inhibition improves obesity-related metabolic dysfunction. *Nat. Commun.* **6**, 10166 (2015).
55. Xie, C. et al. An intestinal farnesoid X receptor-ceramide signaling axis modulates hepatic gluconeogenesis in mice. *Diabetes* **66**, 613–626 (2017).
56. Zhang, X. et al. Adipocyte hypoxia-inducible factor 2 $\alpha$  suppresses atherosclerosis by promoting adipose ceramide catabolism. *Cell Metab.* **30**, 937–951 (2019).
57. Chaurasia, B. et al. Adipocyte ceramides regulate subcutaneous adipose browning, inflammation and metabolism. *Cell Metab.* **24**, 820–834 (2016).
58. Turpin, S. M. et al. Obesity-induced CerS6-dependent C16:0 ceramide production promotes weight gain and glucose intolerance. *Cell Metab.* **20**, 678–686 (2014).
59. Wegner, M. S., Schiffmann, S., Parnham, M. J., Geisslinger, G. & Grosch, S. The enigma of ceramide synthase regulation in mammalian cells. *Prog. Lipid Res.* **63**, 93–119 (2016).
60. Schiffmann, S. et al. Ceramide metabolism in mouse tissue. *Int. J. Biochem. Cell Biol.* **45**, 1886–1894 (2013).
61. Peters, F. et al. Ceramide synthase 4 regulates stem cell homeostasis and hair follicle cycling. *J. Invest. Dermatol.* **135**, 1501–1509 (2015).
62. Mizutani, Y., Kihara, A. & Igarashi, Y. Mammalian Lass6 and its related family members regulate synthesis of specific ceramides. *Biochem. J.* **390**, 263–271 (2005).
63. Whitfield, J. R., Beaulieu, M. E. & Soucek, L. Strategies to inhibit myc and their clinical applicability. *Front Cell Dev. Biol.* **5**, 10 (2017).
64. Guo, J. et al. Efficacy, pharmacokinetics, tissue distribution, and metabolism of the Myc-Max disruptor, 10058-F4 [Z,E]-5-[4-ethylbenzylidene]-2-thioxothiazolidin-4-one, in mice. *Cancer Chemother. Pharmacol.* **63**, 615–625 (2009).
65. de Alboran, I. M. et al. Analysis of C-MYC function in normal cells via conditional gene-targeted mutation. *Immunity* **14**, 45–55 (2001).
66. Madison, B. B. et al. Cis elements of the villin gene control expression in restricted domains of the vertical (crypt) and horizontal (duodenum, cecum) axes of the intestine. *J. Biol. Chem.* **277**, 33275–33283 (2002).
67. el Marjou, F. et al. Tissue-specific and inducible Cre-mediated recombination in the gut epithelium. *Genesis* **39**, 186–193 (2004).
68. Okita, K., Nakagawa, M., Hyenjong, H., Ichisaka, T. & Yamanaka, S. Generation of mouse induced pluripotent stem cells without viral vectors. *Science* **322**, 949–953 (2008).
69. Huang da, W., Sherman, B. T. & Lempicki, R. A. Bioinformatics enrichment tools: paths toward the comprehensive functional analysis of large gene lists. *Nucleic Acids Res.* **37**, 1–13 (2009).
70. Huang da, W., Sherman, B. T. & Lempicki, R. A. Systematic and integrative analysis of large gene lists using DAVID bioinformatics resources. *Nat. Protoc.* **4**, 44–57 (2009).

## Acknowledgements

We thank Q. Wang, D. Lu and J. Zhao for help with animal dissection and sample collection, and L. Byrd for assistance with the mouse protocols. We thank J. M. Sedevy for providing the *Myc<sup>f/f</sup>* mice, D. L. Gumucio for transferring the villin-cre mice and P. Champon for providing the villin-ERT2-cre mice. This study was supported by the National Cancer Institute Intramural Research Program (ZIA BC005562; to F.J.G.) and the Outstanding academic leaders plan of Shanghai (grant no. 2018BR07; to W.L.). S.Y. was supported by a visiting fellowship from the First Affiliated Hospital, University of Science and Technology of China.

## Author contributions

Y.L., S.Y., X.W., L.S. and J.C. performed experiments. K.W.K. helped with the lipidomics analysis. C.X. and X.G. helped with RNA-seq analysis. H.B.D. helped with immunohistochemistry staining. C.J., C.X. and S.T. provided valuable suggestions about experimental design. W.L. collected human ileum biopsies. O.G. helped with indirect calorimetry. Y.L. and F.J.G. were responsible for the study concept and design. Y.L. and F.J.G. wrote the manuscript. W.L. and F.J.G. supervised the study. All authors approved the final version of the manuscript.

## Competing interests

The authors declare no competing interests.

## Additional information

**Extended data** is available for this paper at <https://doi.org/10.1038/s42255-021-00421-8>.

**Supplementary information** The online version contains supplementary material available at <https://doi.org/10.1038/s42255-021-00421-8>.

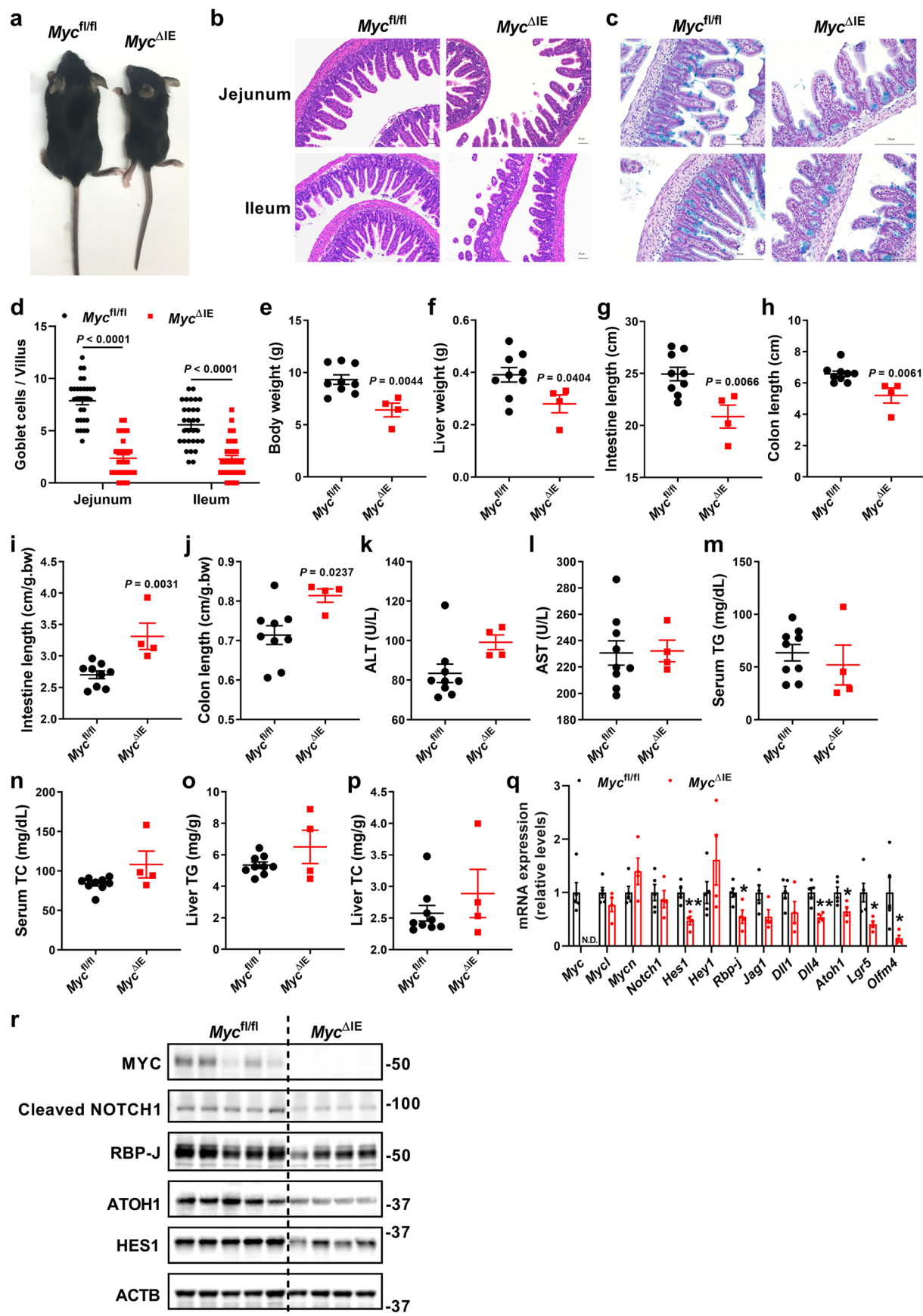
**Correspondence and requests for materials** should be addressed to W.L. or F.J.G.

**Peer review information** *Nature Metabolism* thanks William Holland, Ömer Yilmaz and the other, anonymous, reviewer(s) for their contribution to the peer review of this work. Primary Handling Editor: Christoph Schmitt.

**Reprints and permissions information** is available at [www.nature.com/reprints](http://www.nature.com/reprints).

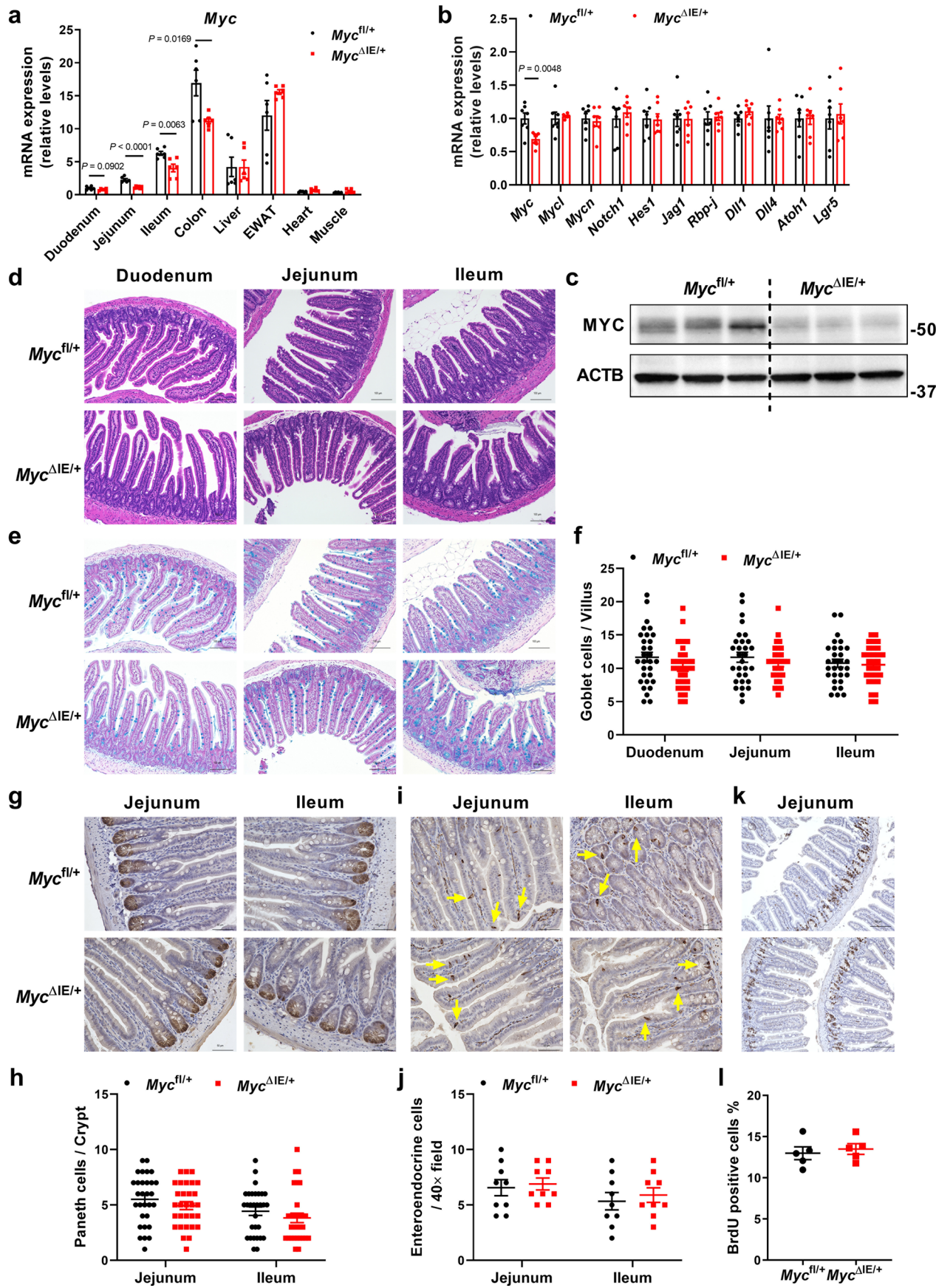
**Publisher's note** Springer Nature remains neutral with regard to jurisdictional claims in published maps and institutional affiliations.

This is a U.S. government work and not under copyright protection in the U.S.; foreign copyright protection may apply 2021



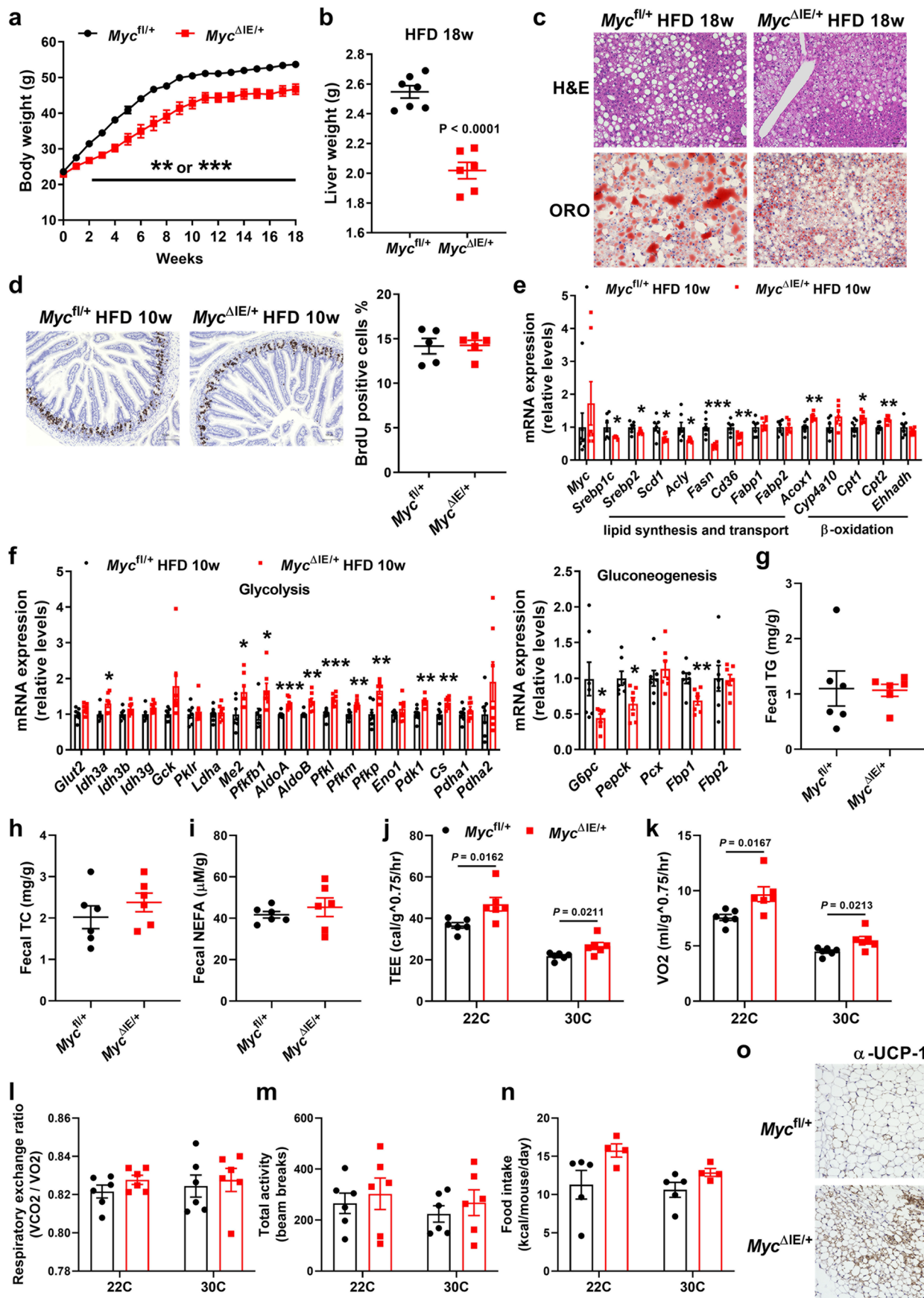
Extended Data Fig. 1 | See next page for caption.

**Extended Data Fig. 1 | Homozygous loss of MYC in the intestine was lethal.** *Myc<sup>f/f</sup>* and *Myc<sup>ΔE</sup>* mice at 21 days of age. **a**, Photos of *Myc<sup>f/f</sup>* and *Myc<sup>ΔE</sup>* mice. **b**, Representative H&E staining of intestine sections ( $n=3$  mice/group, 3 images/mouse). Scale bar, 50  $\mu$ m. **c**, Representative Alcian Blue staining of intestine sections ( $n=3$  mice/group, 3 images/mouse). Scale bar, 100  $\mu$ m. **d**, Number of goblet cells.  $n=30$ . **e**, Body weight. **f**, Liver weight. **g**, Small intestine length. **h**, Colon length. **i**, Small intestine length to body weight ratio. **j**, Colon length to body weight ratio. **k**, Serum ALT. **l**, Serum AST. **m**, Serum triglyceride. **n**, Serum total cholesterol. **o**, Hepatic triglyceride. **p**, Hepatic total cholesterol. **e-p**,  $n=9$  for *Myc<sup>f/f</sup>* mice and  $n=4$  for *Myc<sup>ΔE</sup>* mice. **q**, The mRNA levels of indicated genes in the intestine of *Myc<sup>f/f</sup>* and *Myc<sup>ΔE</sup>* mice.  $n=5$  for *Myc<sup>f/f</sup>* mice and  $n=4$  for *Myc<sup>ΔE</sup>* mice. \* or \*\*  $P=0.0030$ , 0.0167, 0.0040, 0.0402, 0.0235, 0.0344, from left to right. N.D., not detectable. **r**, Western blot analysis of indicated proteins in the intestine of *Myc<sup>f/f</sup>* and *Myc<sup>ΔE</sup>* mice. All data are presented as mean  $\pm$  S.E.M. of biologically independent samples, analyzed using a two-tailed Student's *t*-test (**d-q**).



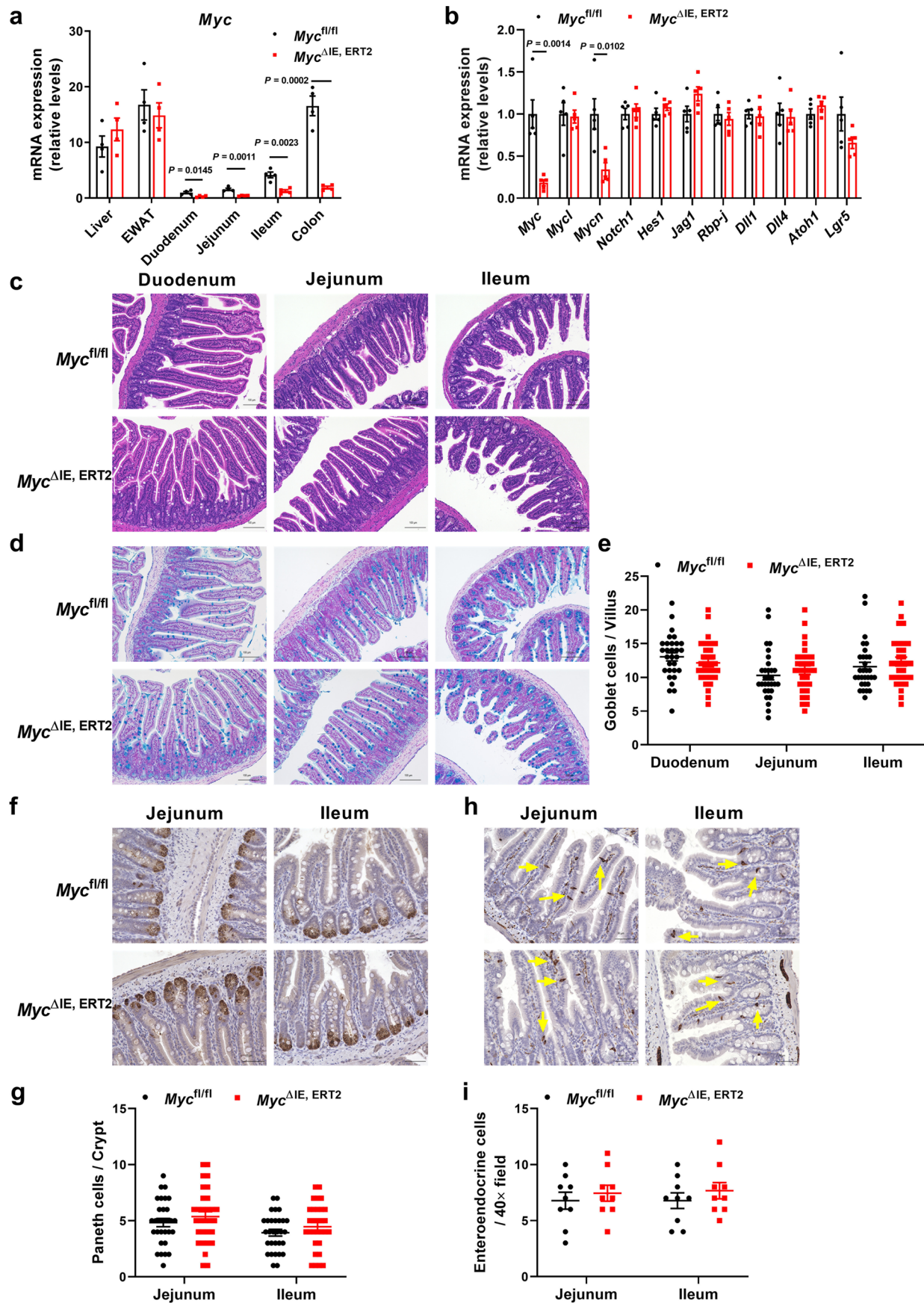
Extended Data Fig. 2 | See next page for caption.

**Extended Data Fig. 2 | Generation of mice with heterozygous loss of MYC in the intestine.** **a**, Myc mRNA levels in different tissues of *Myc*<sup>f/+</sup> and *Myc*<sup>ΔE/+</sup> mice. n = 6. **b**, The mRNA levels of indicated genes in the intestine of *Myc*<sup>f/+</sup> and *Myc*<sup>ΔE/+</sup> mice. n = 7. **c**, The protein levels of MYC in the intestine of *Myc*<sup>f/+</sup> and *Myc*<sup>ΔE/+</sup> mice. **d**, Representative H&E staining of intestine sections (n = 3 mice/group, 3 images/mouse). Scale bar, 100 μm. **e**, Representative Alcian Blue staining of intestine sections (n = 3 mice/group, 3 images/mouse). Scale bar, 100 μm. **f**, Number of goblet cells. n = 30. **g**, Representative immunohistochemistry staining of lysozyme on intestine sections (n = 3 mice/group, 3 images/mouse). Scale bar, 50 μm. **h**, Number of Paneth cells. n = 30. **i**, Representative immunohistochemistry staining of synaptophysin on intestine sections (n = 3 mice/group, 3 images/mouse). Scale bar, 50 μm. **j**, Number of enteroendocrine cells. n = 9. **k**, Representative BrdU staining of intestine sections (n = 5 mice/group, 9 images/mouse). Scale bar, 100 μm. **l**, BrdU labeling index. n = 5. All data are presented as mean ± S.E.M. of biologically independent samples, analyzed using a two-tailed Student's t-test (**a,b,f,h,j,l**).



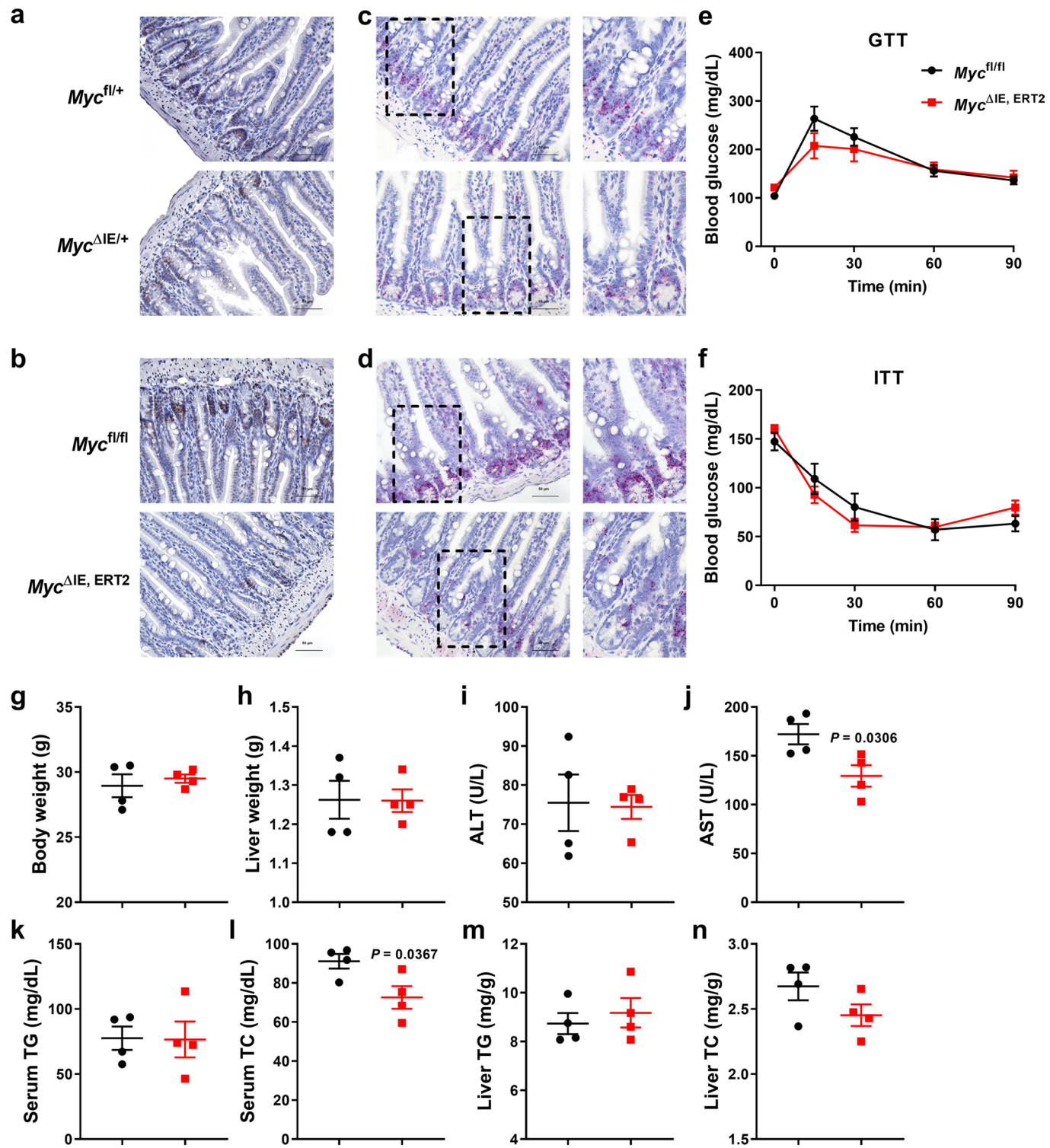
Extended Data Fig. 3 | See next page for caption.

**Extended Data Fig. 3 | Intestinal cell proliferation, hepatic gene expression and energy expenditure of *Myc*<sup>ΔIE/+</sup> mice under HFD.** **a-c**, *Myc*<sup>f/+</sup> and *Myc*<sup>ΔIE/+</sup> mice were fed a HFD for 18 weeks. Representative of  $n=2$  experiments. **a**, Body weight curve. \*\* or \*\*\* $P=0.0003, 0.0002, <0.0001, 0.0008, 0.0009, 0.0008, 0.0008, 0.0008, 0.0007, 0.0010, 0.0004, 0.0003, 0.0005, 0.0003, <0.0001, 0.0004, 0.0004$  from 2w to 18w. **b**, Liver weight. **a,b**,  $n=7$  for *Myc*<sup>f/+</sup> mice and  $n=6$  for *Myc*<sup>ΔIE/+</sup> mice. **c**, Representative H&E and Oil Red O staining of liver sections ( $n=4$  mice/group, 3 images/mouse). Scale bar, 50  $\mu$ m. **d-f**, *Myc*<sup>f/+</sup> and *Myc*<sup>ΔIE/+</sup> mice were fed a HFD for 10 weeks. Representative of  $n=3$  experiments. **d**, Representative BrdU staining of intestine sections ( $n=5$  mice/group, 9 images/mouse). Scale bar, 100  $\mu$ m. right, BrdU labeling index,  $n=5$ . **e**, Hepatic expression of genes involved in lipid synthesis, transport and  $\beta$ -oxidation.  $n=7$ . \* or \*\* or \*\*\*  $P=0.0412, 0.0456, 0.0165, 0.0216, 0.0002, 0.0071, 0.0027, 0.0124, 0.0022$ , from left to right. **f**, Hepatic expression of genes involved in glycolysis (left) and gluconeogenesis (right).  $n=7$ . \* or \*\* or \*\*\*  $P=0.0376, 0.0231, 0.0235, 0.0007, 0.0047, 0.0004, 0.0067, 0.0015, 0.0047, 0.0045, 0.0407, 0.0175, 0.0058$ , from left to right. **g-i**, *Myc*<sup>f/+</sup> and *Myc*<sup>ΔIE/+</sup> mice were fed a HFD for 2 weeks.  $n=6$ . Representative of  $n=3$  experiments. **g**, Fecal triglyceride. **h**, Fecal total cholesterol. **i**, Fecal NEFA. **j-n**, *Myc*<sup>f/+</sup> and *Myc*<sup>ΔIE/+</sup> mice were fed a HFD for 4 weeks. **j**, Total energy expenditure. **k**, Oxygen consumption rate. **l**, Respiratory exchange ratio. **m**, Total activity. **n**, Food intake. **j-m**,  $n=6$ . **n**,  $n=5$  for *Myc*<sup>f/+</sup> and  $n=4$  for *Myc*<sup>ΔIE/+</sup>. **o**, Representative immunohistochemistry staining of UCP-1 on subcutaneous white adipose tissues from *Myc*<sup>f/+</sup> and *Myc*<sup>ΔIE/+</sup> mice fed a HFD for 10 weeks ( $n=3$  mice/group, 3 images/mouse). Scale bar, 50  $\mu$ m. All data are presented as mean  $\pm$  S.E.M. of biologically independent samples, analyzed using a two-tailed Student's *t*-test (**a,b,d-n**).

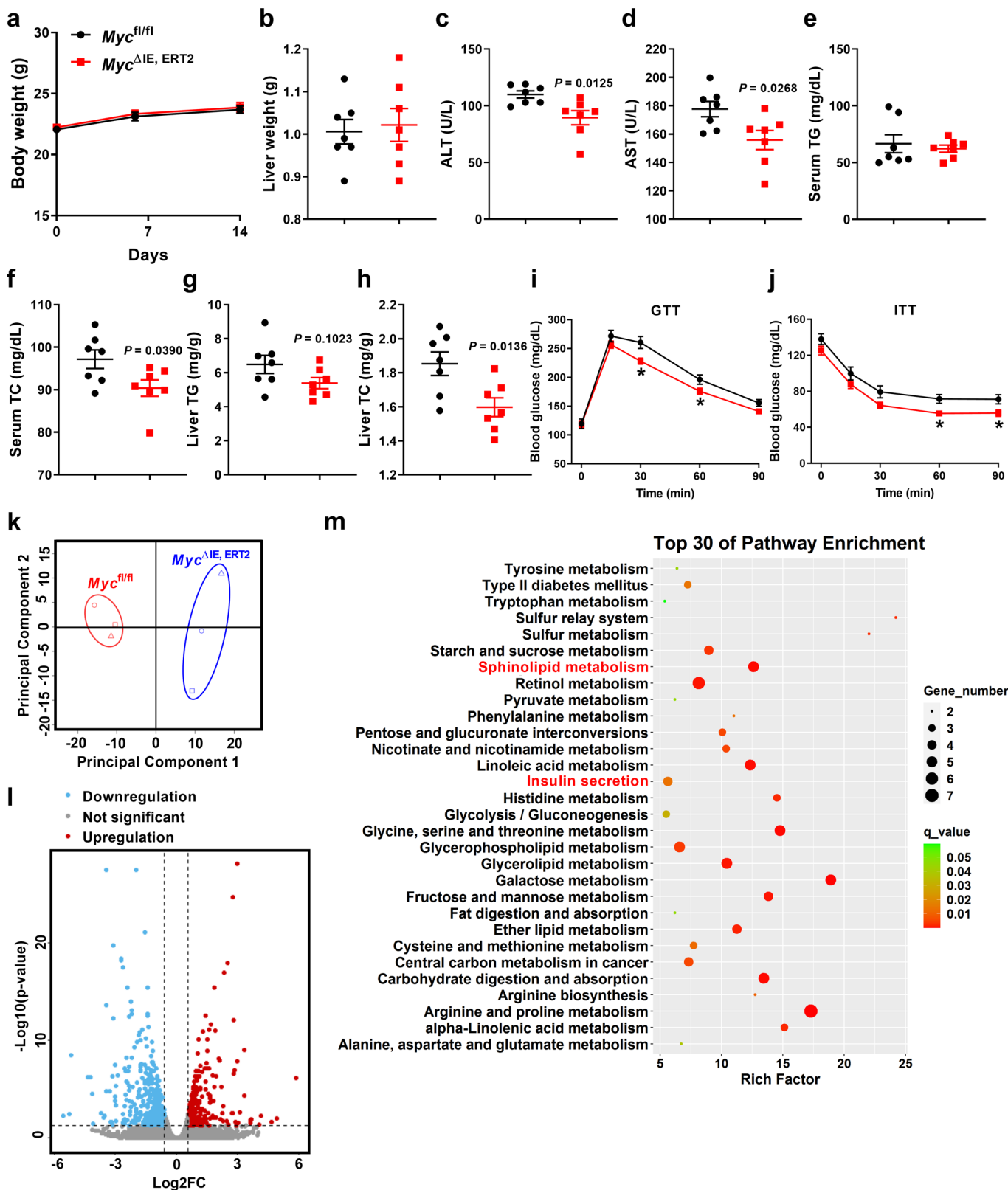


Extended Data Fig. 4 | See next page for caption.

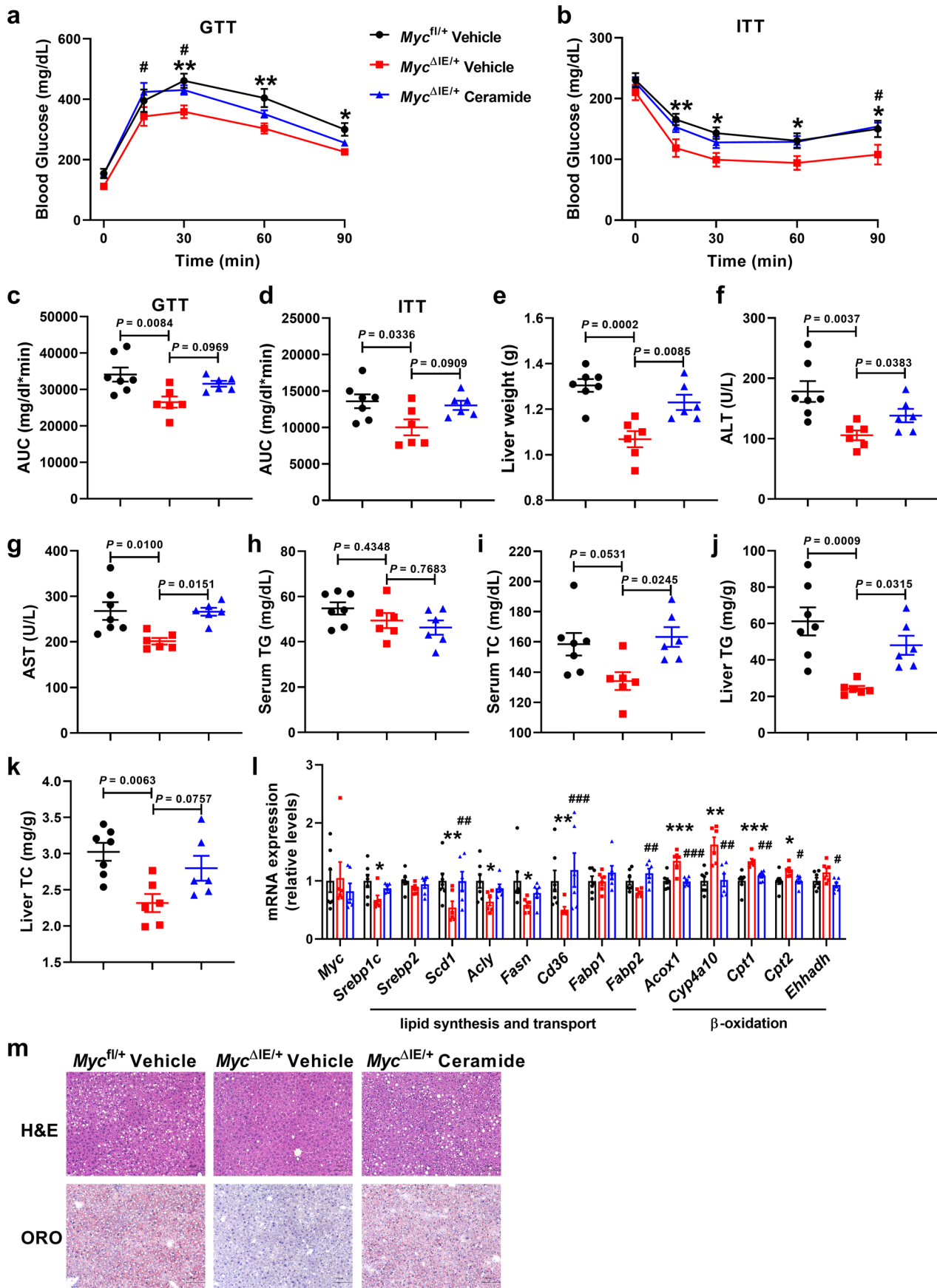
**Extended Data Fig. 4 | Generation of mice with inducible loss of MYC in the intestine.** **a**, Myc mRNA levels in different tissues of  $Myc^{fl/fl}$  and  $Myc^{\Delta IE, ERT2}$  mice treated with tamoxifen.  $n=4$ . **b**, The mRNA levels of indicated genes in the intestine of  $Myc^{fl/fl}$  and  $Myc^{\Delta IE, ERT2}$  mice treated with tamoxifen.  $n=5$ . **c**, Representative H&E staining of intestine sections ( $n=3$  mice/group, 3 images/mouse). Scale bar, 100  $\mu$ m. **d**, Representative Alcian Blue staining of intestine sections ( $n=3$  mice/group, 3 images/mouse). Scale bar, 100  $\mu$ m. **e**, Number of goblet cells.  $n=30$ . **f**, Representative immunohistochemistry staining of lysozyme on intestine sections ( $n=3$  mice/group, 3 images/mouse). Scale bar, 50  $\mu$ m. **g**, Number of Paneth cells.  $n=30$ . **h**, Representative immunohistochemistry staining of synaptophysin on intestine sections ( $n=3$  mice/group, 3 images/mouse). Scale bar, 50  $\mu$ m. **i**, Number of enteroendocrine cells.  $n=9$ . All data are presented as mean  $\pm$  S.E.M. of biologically independent samples, analyzed using a two-tailed Student's *t*-test (**a,b,e,g,i**).



**Extended Data Fig. 5 | Metabolic parameters of Myc<sup>ΔIE, ERT2</sup> mice under chow diet.** **a**, Representative immunohistochemistry staining of MYC on intestine sections from Myc<sup>fl/fl</sup> and Myc<sup>ΔIE/+</sup> mice ( $n=3$  mice/group, 3 images/mouse). Scale bar, 50  $\mu$ m. **b**, Representative immunohistochemistry staining of MYC on intestine sections from Myc<sup>fl/fl</sup> and Myc<sup>ΔIE, ERT2</sup> mice ( $n=3$  mice/group, 3 images/mouse). Scale bar, 50  $\mu$ m. **c**, Representative *in situ* hybridization of Myc on intestine sections from Myc<sup>fl/fl</sup> and Myc<sup>ΔIE/+</sup> mice ( $n=2$  mice/group, 3 images/mouse). Scale bar, 50  $\mu$ m. **d**, Representative *in situ* hybridization of Myc on intestine sections from Myc<sup>fl/fl</sup> and Myc<sup>ΔIE, ERT2</sup> mice ( $n=2$  mice/group, 3 images/mouse). Scale bar, 50  $\mu$ m. **e–n**, Myc<sup>fl/fl</sup> and Myc<sup>ΔIE, ERT2</sup> mice were weekly injected with tamoxifen for 6 weeks from 8 weeks of age. **e**, Glucose tolerance test. **f**, Insulin tolerance test. **g**, Body weight. **h**, Liver weight. **i**, Serum ALT. **j**, Serum AST. **k**, Serum triglyceride. **l**, Serum total cholesterol. **m**, Hepatic triglyceride. **n**, Hepatic total cholesterol. **e–n**,  $n=4$ . All data are presented as mean  $\pm$  S.E.M. of biologically independent samples, analyzed using a two-tailed Student's *t*-test (**e–n**).

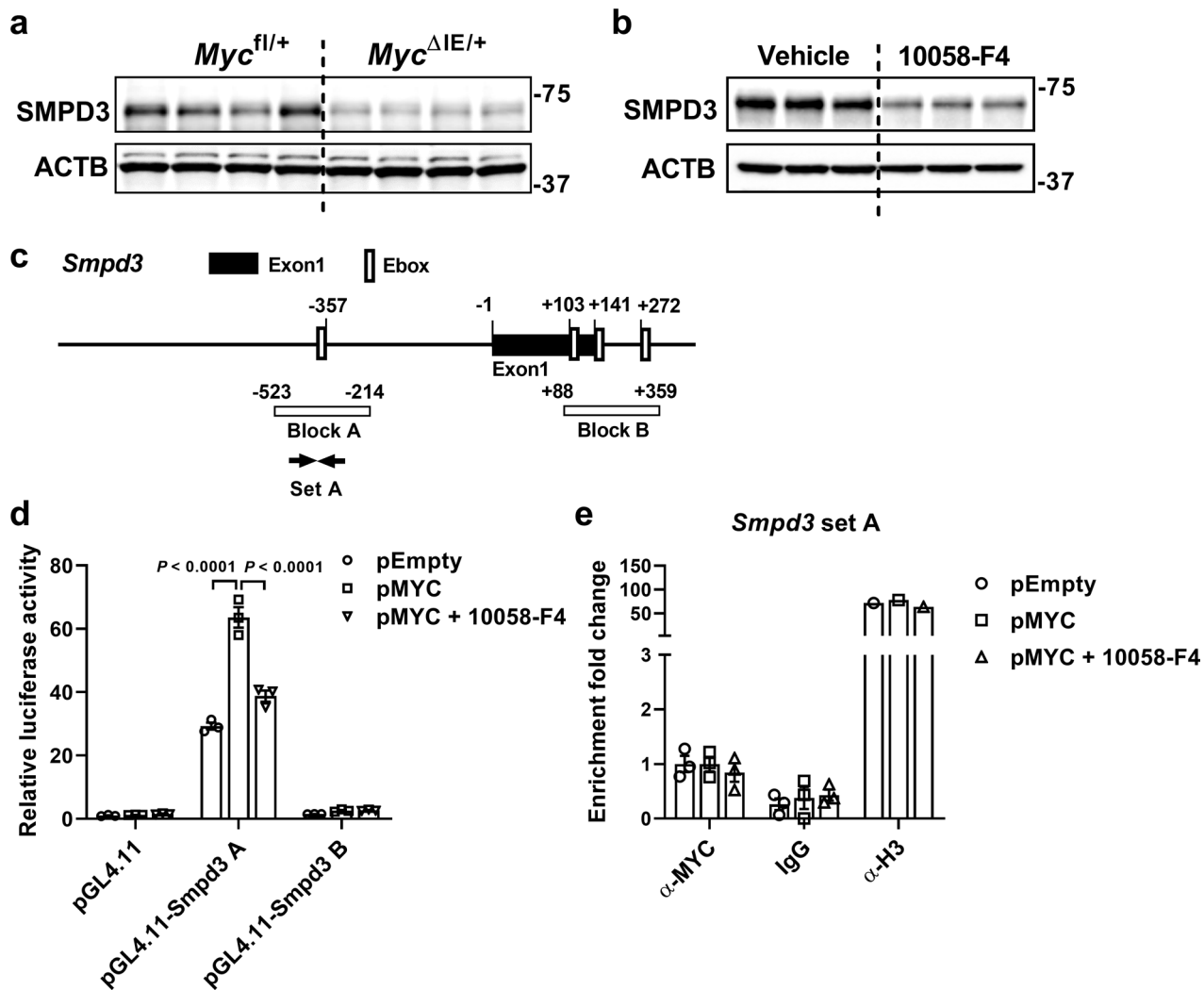


**Extended Data Fig. 6 | RNA-seq analysis of Myc<sup>ΔIE, ERT2</sup> mice fed a HFD for 2 weeks.** **a-j.** Myc<sup>fl/fl</sup> and Myc<sup>ΔIE, ERT2</sup> mice were injected with tamoxifen and fed a HFD for 2 weeks. **a,** Body weight curve. **b,** Liver weight. **c,** Serum ALT. **d,** Serum AST. **e,** Serum triglyceride. **f,** Serum total cholesterol. **g,** Hepatic triglyceride. **h,** Hepatic total cholesterol. **a-h,** n = 7. **i,j,** Glucose tolerance test. **j,** Insulin tolerance test. **i,j,** n = 9 for Myc<sup>fl/fl</sup> mice and n = 10 for Myc<sup>ΔIE, ERT2</sup> mice. \*P = 0.0113 (GTT, 30 min), 0.0497 (GTT, 60 min), 0.0103 (ITT, 60 min), 0.0224 (ITT, 90 min). All data are presented as mean ± S.E.M. of biologically independent samples, analyzed using a two-tailed Student's t-test (**a-j**). The PCA plot (**k**), volcano plot (**l**) and pathway enrichment (**m**) of the RNA-seq data from the intestines of Myc<sup>fl/fl</sup> and Myc<sup>ΔIE, ERT2</sup> mice injected with tamoxifen and fed a HFD for 2 weeks.

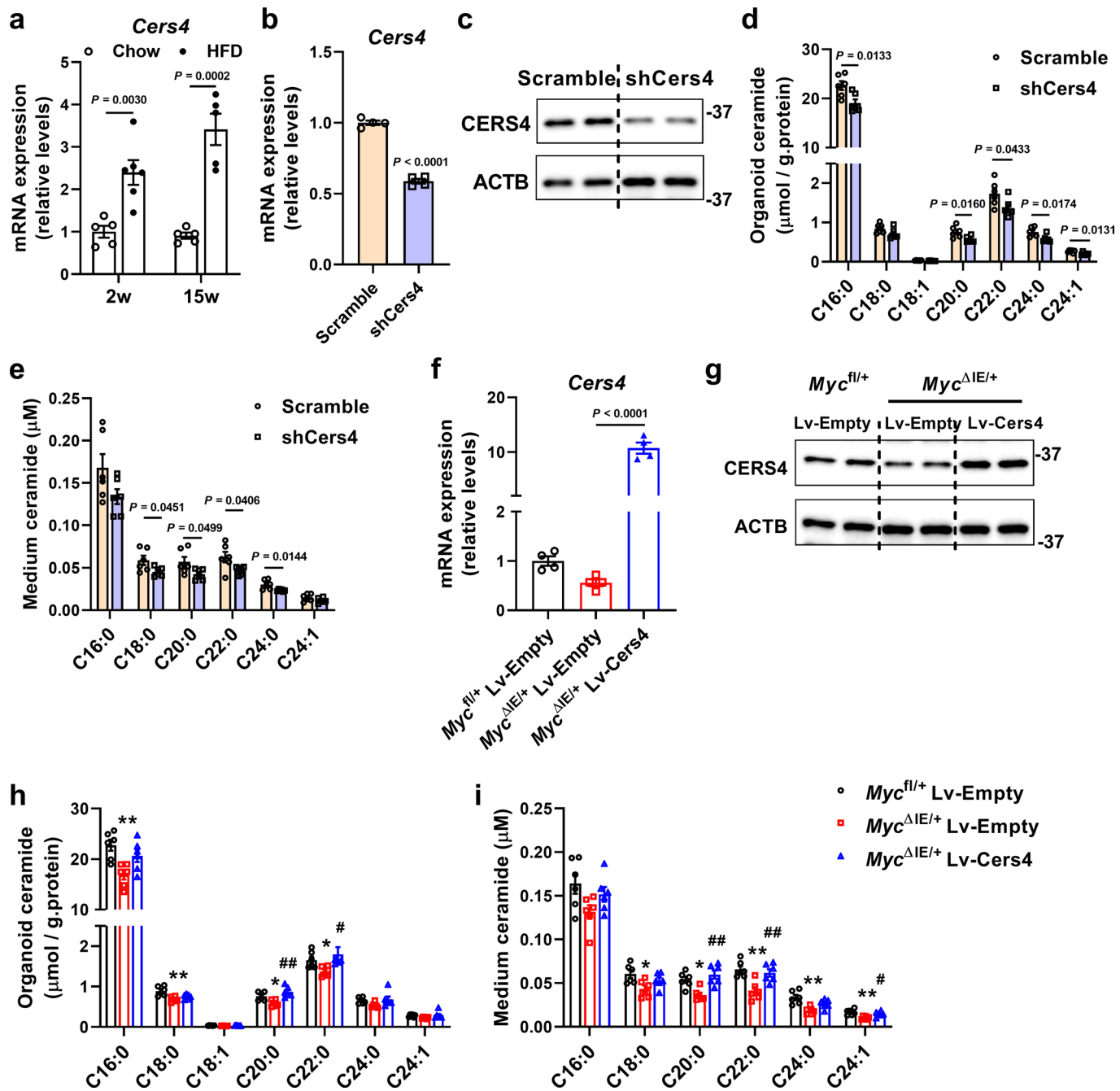


Extended Data Fig. 7 | See next page for caption.

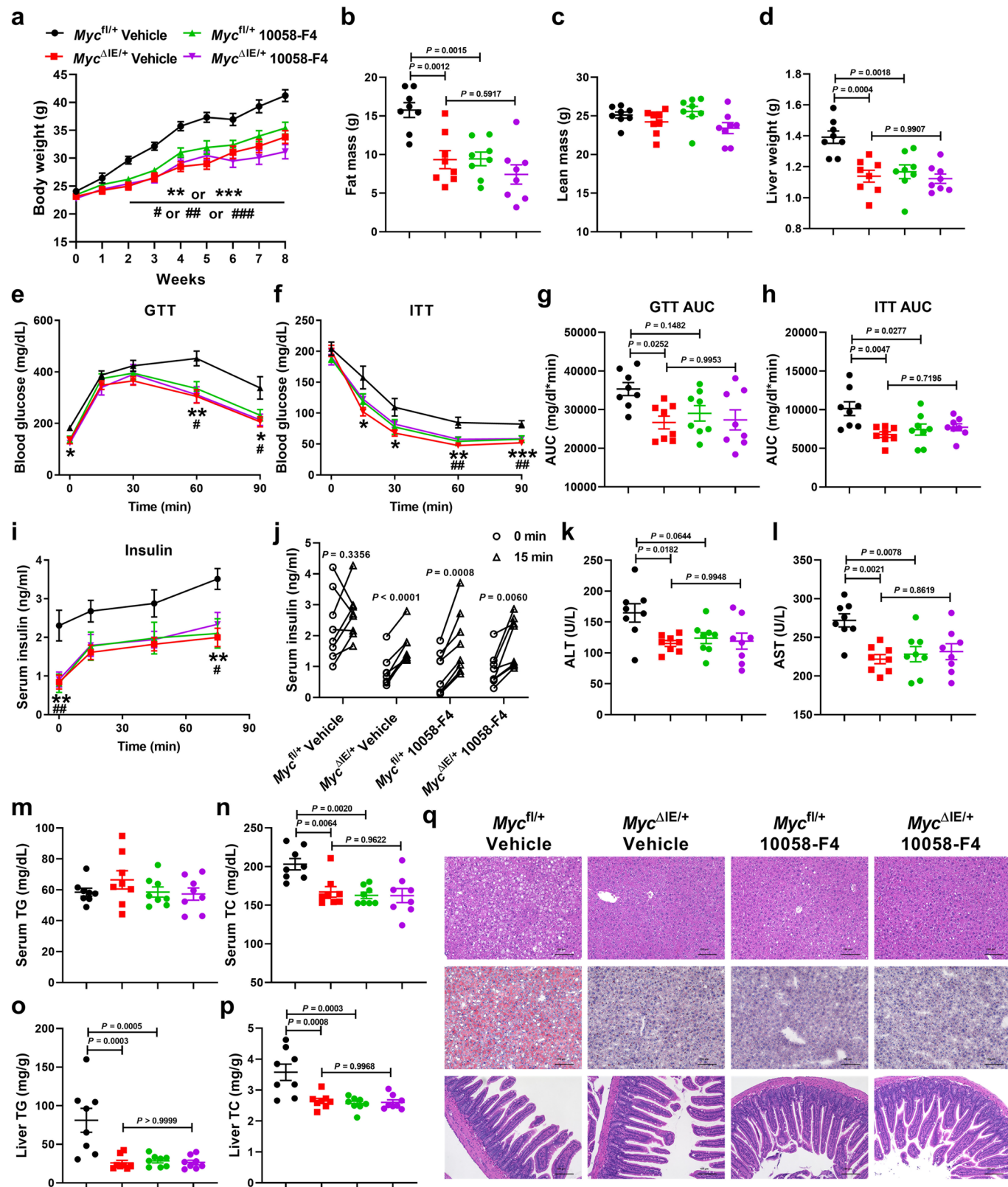
**Extended Data Fig. 7 | Intestinal Myc disruption improved obesity and fatty liver through ceramide reduction.** *Myc<sup>fl/+</sup>* and *Myc<sup>ΔE/+</sup>* mice were fed a HFD and daily i.p. injected with vehicle or ceramide for 6 weeks. Representative of n=2 experiments. **a**, Glucose tolerance test. **b**, Insulin tolerance test. **a,b**, \* or \*\*P=0.0027, 0.0031, 0.0340, 0.0074, 0.0139, 0.0428, 0.0179, from left to right, *Myc<sup>ΔE/+</sup>* Vehicle group versus *Myc<sup>fl/+</sup>* Vehicle group. # or ##P=0.0138, 0.0341, 0.0120, from left to right, *Myc<sup>ΔE/+</sup>* Ceramide group versus *Myc<sup>ΔE/+</sup>* Vehicle group. **c**, GTT AUC. **d**, ITT AUC. **e**, Liver weight. **f**, Serum ALT. **g**, Serum AST. **h**, Serum triglyceride. **i**, Serum total cholesterol. **j**, Hepatic triglyceride. **k**, Hepatic total cholesterol. **l**, The mRNA levels of indicated genes in the liver. \* or \*\* or \*\*\*P=0.0325, 0.0062, 0.0383, 0.0145, 0.0027, 0.0007, 0.0013, 0.0005, 0.0319, from left to right, *Myc<sup>ΔE/+</sup>* Vehicle group versus *Myc<sup>fl/+</sup>* Vehicle group. # or ## or ###P=0.0091, <0.0001, 0.0059, 0.0007, 0.0023, 0.0089, 0.0345, 0.0477, from left to right, *Myc<sup>ΔE/+</sup>* Ceramide group versus *Myc<sup>ΔE/+</sup>* Vehicle group. **a-l**, n=7 for *Myc<sup>fl/+</sup>* Vehicle group. n=6 for *Myc<sup>ΔE/+</sup>* Vehicle group and *Myc<sup>ΔE/+</sup>* Ceramide group. All data are presented as mean ± S.E.M. of biologically independent samples, analyzed using one-way ANOVA followed by Tukey's multiple comparisons test (**c-l**), or two-way ANOVA followed by Dunnett's multiple comparisons test (**a,b**). **m**, Representative H&E and Oil Red O staining of liver sections (n=4 mice/group, 3 images/mouse). Scale bar, 100 μm.



**Extended Data Fig. 8 | Intestinal Myc disruption decreased SMPD3 levels.** **a**, Protein levels of SMPD3 in the intestine of *Myc<sup>fl/+</sup>* and *Myc<sup>ΔIE/+</sup>* mice fed a HFD for 2 weeks. **b**, Protein levels of SMPD3 in the intestine of C57BL/6N mice first fed a HFD for 6 weeks and then daily gavaged with vehicle or 50 mg/kg 10058-F4 while maintained on a HFD for another 8 weeks. **c**, Schematic diagram of the mouse *Smpd3* promoter illustrating the predicted Ebox sites in the regulatory region and the fragments used for the luciferase reporter assay. **d**, Luciferase reporter assay of the mouse *Smpd3* promoter activity. n=3. **e**, ChIP assay with MC38 cells transfected with empty backbone or MYC overexpression plasmid and treated with vehicle or 40 μM 10058-F4 for 48 h. n=3 for α-MYC and IgG groups, n=1 for α-H3 group. All data are presented as mean ± S.E.M. of biologically independent samples, analyzed using two-way ANOVA followed by Tukey's multiple comparisons test (**d,e**).



**Extended Data Fig. 9 | CERS4 regulated ceramide production in intestinal organoids.** **a**, Cers4 mRNA levels in the intestine of C57BL/6 N mice fed a chow diet or HFD for 2 weeks or 15 weeks. n=5 for 2w chow, 15w chow and 15w HFD. n=6 for 2w HFD. **b-e**, Intestinal organoids were isolated from Myc<sup>fl/+</sup> mice fed a HFD for 2 weeks and infected with lentiviruses carrying scramble siRNA (scramble) or Cers4 shRNA (shCers4). **b**, Cers4 mRNA levels in intestinal organoids. n=6. **c**, CERS4 protein levels in intestinal organoids. **d**, Ceramide levels in the intestinal organoids. n=6. **e**, Ceramide levels in the culture medium of intestinal organoids. n=6. **f-i**, Intestinal organoids were isolated from Myc<sup>fl/+</sup> and Myc<sup>ΔIE/+</sup> mice fed a HFD for 2 weeks and infected with control lentiviruses (Lv-Empty) or lentiviruses carrying Cers4 cDNA (Lv-Cers4). **f**, Cers4 mRNA levels in intestinal organoids. n=4. **g**, CERS4 protein levels in intestinal organoids. **h**, Ceramide levels in the intestinal organoids. n=6. **i**, Ceramide levels in the culture medium of intestinal organoids. n=6. **h-i**, \* or \*\* P = 0.0046, 0.0016, 0.0309, 0.0229, 0.0212, 0.0136, 0.0018, 0.0012, 0.0031, from left to right, Myc<sup>ΔIE/+</sup> Lv-Empty group versus Myc<sup>fl/+</sup> Lv-Empty group. # or ## P = 0.0012, 0.0492, 0.0015, 0.0072, 0.0416, from left to right, Myc<sup>ΔIE/+</sup> Lv-Cers4 group versus Myc<sup>ΔIE/+</sup> Lv-Empty group. All data are presented as mean  $\pm$  S.E.M. of biologically independent samples, analyzed using a two-tailed Student's t-test (**a,b,d,e**), or one-way ANOVA followed by Tukey's multiple comparisons test (**f,h,i**).



Extended Data Fig. 10 | See next page for caption.

**Extended Data Fig. 10 | The effect of 10058-F4 on metabolic syndrome was dependent on intestinal MYC.** *Myc<sup>f/f</sup>* and *Myc<sup>ΔE/+</sup>* mice were fed a HFD and treated with vehicle or 10058-F4 for 8 weeks. **a**, Body weight curve. \*\* or \*\*\*P=0.0013 for 2w, <0.0001 for 3–8w, *Myc<sup>ΔE/+</sup>* Vehicle group versus *Myc<sup>f/f</sup>* Vehicle group. # or ## or ###P=0.0307, 0.0033, 0.0011, 0.0001, 0.0015, 0.0001, <0.0001 for 2–8w, *Myc<sup>f/f</sup>* 10058-F4 group versus *Myc<sup>f/f</sup>* Vehicle group. **b**, Fat mass. **c**, Lean mass. **d**, Liver weight. **e**, Glucose tolerance test. **f**, Insulin tolerance test. **g**, GTT AUC. **h**, ITT AUC. **i**, Insulin curve in response to glucose. \*\*P=0.0031 (0 min), 0.0078 (75 min), *Myc<sup>ΔE/+</sup>* Vehicle group versus *Myc<sup>f/f</sup>* Vehicle group. # or ##P=0.0025 (0 min), 0.0140 (75 min), *Myc<sup>f/f</sup>* 10058-F4 group versus *Myc<sup>f/f</sup>* Vehicle group. **j**, insulin levels at 0 min and 15 min post glucose load. **k**, Serum ALT. **l**, Serum AST. **m**, Serum triglyceride. **n**, Serum total cholesterol. **o**, Hepatic triglyceride. **p**, Hepatic total cholesterol. **a–p**, n=8. All data are presented as mean ± S.E.M. of biologically independent samples, analyzed using one-way ANOVA followed by Tukey's multiple comparisons test (**b–d,g,h,k–p**), two-way ANOVA followed by Tukey's multiple comparisons test (**a,e,f,i**), or a two-tailed paired t-test (**j**). **q**, Representative H&E staining of liver (top) and intestine sections (bottom), and Oil Red O staining of liver sections (middle) (n=4 mice/group, 3 images/mouse). Scale bar, 100 μm.

## Reporting Summary

Nature Research wishes to improve the reproducibility of the work that we publish. This form provides structure for consistency and transparency in reporting. For further information on Nature Research policies, see our [Editorial Policies](#) and the [Editorial Policy Checklist](#).

### Statistics

For all statistical analyses, confirm that the following items are present in the figure legend, table legend, main text, or Methods section.

n/a Confirmed

- The exact sample size ( $n$ ) for each experimental group/condition, given as a discrete number and unit of measurement
- A statement on whether measurements were taken from distinct samples or whether the same sample was measured repeatedly
- The statistical test(s) used AND whether they are one- or two-sided  
*Only common tests should be described solely by name; describe more complex techniques in the Methods section.*
- A description of all covariates tested
- A description of any assumptions or corrections, such as tests of normality and adjustment for multiple comparisons
- A full description of the statistical parameters including central tendency (e.g. means) or other basic estimates (e.g. regression coefficient) AND variation (e.g. standard deviation) or associated estimates of uncertainty (e.g. confidence intervals)
- For null hypothesis testing, the test statistic (e.g.  $F$ ,  $t$ ,  $r$ ) with confidence intervals, effect sizes, degrees of freedom and  $P$  value noted  
*Give P values as exact values whenever suitable.*
- For Bayesian analysis, information on the choice of priors and Markov chain Monte Carlo settings
- For hierarchical and complex designs, identification of the appropriate level for tests and full reporting of outcomes
- Estimates of effect sizes (e.g. Cohen's  $d$ , Pearson's  $r$ ), indicating how they were calculated

*Our web collection on [statistics for biologists](#) contains articles on many of the points above.*

### Software and code

Policy information about [availability of computer code](#)

Data collection

Illumina HiSeq4000 was used to collect RNA-seq data.

Data analysis

For RNA-seq data analysis, reads of the samples were trimmed for adapters and low-quality bases using Trimmomatic 0.36 software before alignment with the reference genome (Mouse - mm10) and the annotated transcripts using STAR 2.5.1. The mapping statistics were calculated using Picard 1.84 software. Library complexity was measured in terms of unique fragments in the mapped reads using Picard's MarkDuplicates utility. The gene expression quantification analysis was performed for all samples using STAR/RSEM 1.2.22 tools. Differential gene expression was assessed with DESeq2 with the parameters P-adj 0.05 and log2 fold 0.585 (for 1.5-fold differentially expressed genes). Functional enrichment analysis was performed with DAVID using the pathways related to metabolism from the KEGG database annotation.

For serum global lipidomics, the multivariate data matrix was analyzed by SIMCA-P+15 software (Umetrics, Kinnelon, NJ). For ceramide quantitation, the data were analyzed by TargetLynx software, a subroutine of the MassLynx V4.2 software (Waters Corp.).

Statistical analysis was performed using Prism version 8.4.3 (GraphPad Software, San Diego, CA). Experimental values are presented as mean  $\pm$  S.E.M. Statistical significance between two groups was determined using two-tailed Student's t-test. For comparing insulin levels at 15 min with those at 0 min, two-tailed paired t-test was performed. One-way ANOVA followed by Tukey's multiple comparisons test, or two-way ANOVA followed by Tukey's or Dunnett's multiple comparisons test was applied for multi-group comparisons, as indicated in specific figure legends. Correlations were assessed by nonparametric Spearman's test. P values were calculated with confidence intervals of 95%, and differences were considered statistically significant at  $P < 0.05$ .

For manuscripts utilizing custom algorithms or software that are central to the research but not yet described in published literature, software must be made available to editors and reviewers. We strongly encourage code deposition in a community repository (e.g. GitHub). See the Nature Research [guidelines for submitting code & software](#) for further information.

## Data

Policy information about [availability of data](#)

All manuscripts must include a [data availability statement](#). This statement should provide the following information, where applicable:

- Accession codes, unique identifiers, or web links for publicly available datasets
- A list of figures that have associated raw data
- A description of any restrictions on data availability

Transcriptomic data have been deposited in GEO under accession code GSE155460. Source data are provided with this paper.

## Field-specific reporting

Please select the one below that is the best fit for your research. If you are not sure, read the appropriate sections before making your selection.

Life sciences       Behavioural & social sciences       Ecological, evolutionary & environmental sciences

For a reference copy of the document with all sections, see [nature.com/documents/nr-reporting-summary-flat.pdf](https://nature.com/documents/nr-reporting-summary-flat.pdf)

## Life sciences study design

All studies must disclose on these points even when the disclosure is negative.

|                 |   |
|-----------------|---|
| Sample size     | No statistical tool was used to predetermine sample sizes. Number of biological replicates was determined based on experimental approach, availability of materials and estimates of variances based on our previous experience with similar in vitro and in vivo studies (PMID:29035368, 26670557,25500885).   |
| Data exclusions | No data excluded from analysis.   |
| Replication     | All data were replicated in at least two independent experiments, except RNA-seq analysis and data generated with human ileum biopsies. all attempts at replication were successful. For human ileum biopsies, we only collected one cohort of samples, but the sample size was sufficient to demonstrate statistical significance.   |
| Randomization   | Mice used for studies were selected randomly from a set of genotyped animals. Cohorts were organized between mice weaned together and data collected without exclusion. For MYC inhibitor animal experiment, mice were randomized to treatment group and control group.   |
| Blinding        | The investigators involved in this study were blinded in the clinical sample collections and analyses. For animal studies, investigators and cores performing histology analyses were blind to group allocation. For most of the other experiments, we were unable to set-up blind experiments since the same individual maintaining the mice or cells was also performing the experiment and analysis. |

## Reporting for specific materials, systems and methods

We require information from authors about some types of materials, experimental systems and methods used in many studies. Here, indicate whether each material, system or method listed is relevant to your study. If you are not sure if a list item applies to your research, read the appropriate section before selecting a response.

### Materials & experimental systems

|                                     |   |
|-------------------------------------|---|
| n/a                                 | Involved in the study   |
| <input type="checkbox"/>            | <input checked="" type="checkbox"/> Antibodies                  |
| <input type="checkbox"/>            | <input checked="" type="checkbox"/> Eukaryotic cell lines       |
| <input checked="" type="checkbox"/> | <input type="checkbox"/> Palaeontology and archaeology          |
| <input type="checkbox"/>            | <input checked="" type="checkbox"/> Animals and other organisms |
| <input type="checkbox"/>            | <input checked="" type="checkbox"/> Human research participants |
| <input checked="" type="checkbox"/> | <input type="checkbox"/> Clinical data                          |
| <input type="checkbox"/>            | <input type="checkbox"/> Dual use research of concern           |

### Methods

|                                     |   |
|-------------------------------------|---|
| n/a                                 | Involved in the study                           |
| <input checked="" type="checkbox"/> | <input type="checkbox"/> ChIP-seq               |
| <input checked="" type="checkbox"/> | <input type="checkbox"/> Flow cytometry         |
| <input checked="" type="checkbox"/> | <input type="checkbox"/> MRI-based neuroimaging |

## Antibodies

### Antibodies used

The following primary antibodies were used [primary antibody (cat number, company) (dilution)]:  
 Mouse monoclonal MYC (C-8) (sc-41, Santa Cruz Biotechnology) (1:500 for WB)  
 Rabbit polyclonal CERS4 (ab66512, Abcam) (1:1000 for WB)  
 Rabbit polyclonal ChREBP (ab92809, Abcam) (1:1000 for WB)  
 Rabbit monoclonal ACTB (13E5) (# 4970, Cell Signaling) (1:1000 for WB)  
 Rabbit monoclonal cleaved NOTCH1 (Val1744) (#4147, Cell Signaling) (1:1000 for WB)  
 Rabbit monoclonal RBP-J (D10A4) (#5313, Cell Signaling) (1:1000 for WB)

Rabbit polyclonal ATOH1 (21215-1-AP, Proteintech) (1:1000 for WB)  
 Mouse monoclonal HES1 (E-5) (sc-166410, Santa Cruz Biotechnology) (1:500 for WB)  
 Mouse monoclonal SMPD3 (G-6) (sc-166637, Santa Cruz Biotechnology) (1:500 for WB)

Rabbit polyclonal MYC (# 9402, Cell Signaling) (1:50 for ChIP)  
 Rabbit monoclonal Histone H3 (D2B12) (#4620, Cell Signaling) (1:100 for ChIP)  
 Normal Rabbit IgG (#2729, Cell Signaling) (1:100 for ChIP)

Rabbit polyclonal MYC (ab39688, Abcam) (1:200 for IHC)  
 Rabbit polyclonal lysozyme (EC3.2.1.17, Dako) (1:1000 for IHC)  
 Rabbit monoclonal synaptophysin (SP11) (MA5-14532, Thermo) (1:25 for IHC)  
 Rabbit polyclonal UCP-1 (ab10983, Abcam) (1:500 for IHC)

## Validation

All the antibodies used in this study are commercially available and were used for the applications validated by the manufacturers. Validation procedures are described on the websites of the manufacturers:

Anti-MYC (C-8): Applications: WB, IP, IF and ELISA. Reactivity: Mouse, Rat, Human and Avian.

Anti-CERS4: Applications: WB. Reactivity: Mouse.

Anti-CHREBP: Applications: IHC-P, WB, ICC/IF. Reactivity: Mouse, Human.

Anti-ACTB: Applications: WB, IHC, IF, Flow cytometry. Reactivity: Human, Mouse, Rat, Monkey, Bovine, Pig.

Anti-cleaved NOTCH1: Applications: WB, IP, ChIP. Reactivity: Human, Mouse, Rat.

Anti-RBP-J: Applications: WB, IHC, ChIP. Reactivity: Human, Mouse, Rat, Monkey.

Anti-ATOH1: Applications: Reactivity: WB, IF. Human, Mouse, Rat.

Anti-HES1: Applications: WB, IP, IF, IHC(P), ELISA. Reactivity: Human, Mouse, Rat.

Anti-SMPD3: Applications: WB, IP, IF, IHC(P). Reactivity: Mouse, rat and human.

Anti-MYC (#9402, cell signaling): Applications: WB, IP, ChIP. Reactivity: Human, Mouse, Rat.

Anti-H3: Applications: ChIP. Reactivity: Human, Mouse.

Normal Rabbit IgG: Applications: IP, ChIP.

Anti-MYC (ab39688, abcam): Applications: WB, IHC-P. Reactivity: Mouse, Human.

Anti-lysozyme: Applications: WB, IHC, ICC. Reactivity: Human, Mouse.

Anti-synaptophysin: Applications: WB, IHC, ICC/IF. Reactivity: Human, Mouse, Rat.

Anti-UCP-1: Applications: WB, IHC-P. Reactivity: Mouse, Rat.

## Eukaryotic cell lines

Policy information about [cell lines](#)

|  |  |
|--|--|
| Cell line source(s)  | MC38 was obtained from James W. Hodge, PhD, MBA, National Cancer Institute/NIH.  |
| Authentication   | MC38 cell line obtained from prof. Hodge is already authenticated using STR profiling.   |
| Mycoplasma contamination   | MC38 cell line was maintained under the recommended culture conditions and media requirements. Mycoplasma detection was performed in accordance with department protocols (and tested negative). |
| Commonly misidentified lines<br>(See <a href="#">ICLAC</a> register) | None.  |

## Animals and other organisms

Policy information about [studies involving animals; ARRIVE guidelines](#) recommended for reporting animal research

|                         |   |
|-------------------------|---|
| Laboratory animals      | Mice were maintained in a temperature-controlled room at 20-24°C and average humidity at 40% under a standard 12-h light/12-h dark cycle with water and food provided ad libitum. Myc floxed (Mycfl/fl or Mycfl/+), intestine-specific Myc knockout (MycΔIE, ERT2 or MycΔIE/+), villin-cre, villin-ert2-cre mice were maintained in C57BL/6 background. villin-cre and villin-ert2-cre mice were only used for breeding. All experiments were conducted on male Myc floxed mice, intestine-specific Myc knockout mice and C57BL/6 mice between 7-8 weeks old. |
| Wild animals            | All the studies did not involve wild animals.   |
| Field-collected samples | All the studies did not involve samples collected from the field.   |
| Ethics oversight        | All animal studies and procedures were carried out in accordance with the Institute of Laboratory Animal Care international guidelines and approved by the National Cancer Institute Animal Care and Use Committee.   |

Note that full information on the approval of the study protocol must also be provided in the manuscript.

## Human research participants

Policy information about [studies involving human research participants](#)

|                            |  |
|----------------------------|--|
| Population characteristics | The mucosal biopsies of the distal ileum were taken from individuals with or without obesity. The genders and ages were at |
|----------------------------|--|

|                            |   |
|----------------------------|---|
| Population characteristics | similar levels in obese group ( $BMI \geq 25$ , n = 16) and non-obese group ( $BMI < 25$ , n = 28), with clinical variables listed in Supplementary Table 2.  |
| Recruitment                | The mucosal biopsies of the distal ileum were taken from individuals who were not diagnosed with inflammatory bowel disease or colorectal cancer during routine colonoscopy. All the individuals met the following inclusion criteria: (i) no inflammatory bowel disease; (ii) no colorectal cancer; (iii) no colorectal polyps; (iv) no acute or chronic viral hepatitis; (v) no pregnancy; (vi) no alcoholic liver disease or daily drinking habits; (vii) no disease judged by clinicians as unsuitable for biopsy. There was no self-selection or other bias. |
| Ethics oversight           | The study was approved by the Ethics Committee of Shanghai Tenth People's Hospital, and all patients were given written informed consent before participating in the study.   |

Note that full information on the approval of the study protocol must also be provided in the manuscript.